Redox Biology 56 (2022) 102441

Contents lists available at ScienceDirect

Redox Biology

journal homepage: www.elsevier.com/locate/redox

# $Mo_3Se_4$ nanoparticle with ROS scavenging and multi-enzyme activity for the treatment of DSS-induced colitis in mice

Hongrui Guo [a,1], Hai Guo [b,1], Yue Xie [a], Yinyin Chen [c], Changfang Lu [b], Zhouping Yang [b], Yanqiu Zhu [a], Yujuan Ouyang [a], Yu Zhang [d], Xianxiang Wang [b,*]

[a] College of Veterinary Medicine, Sichuan Agricultural University, Chengdu, 611130, Sichuan, China
[b] College of Science, Sichuan Agricultural University, Chengdu, 611130, Sichuan, China
[c] College of Agronomy, Sichuan Agricultural University, Chengdu, 611130, Sichuan, China
[d] State Key Laboratory of Hybrid Rice, Rice Research Institute, Sichuan Agricultural University, Chengdu, 611130, China

ARTICLE INFO

*Keywords:*
Ulcerative colitis
$Mo_3Se_4$ nanozyme
Inflammation
Oxidative stress
Intestinal barrier

ABSTRACT

Ulcerative colitis (UC), as a most common inflammatory bowel disease (IBD), has become a global public health concern. Exploring novel method of treating UC is urgent and necessary. Recently, nanozyme with excellent antioxidant properties may be one useful therapeutic strategy. In this study, a two-dimensional transition metal chalcogenide (TMCs) nano flake and polyethylene glycol (PEG) modified $Mo_3Se_4$ nano flakes (PMNFs) was synthesized, which had multi-enzyme activity, including peroxidase, glutathione peroxidase (GPx), superoxide dismutase (SOD), and catalase (CAT). The inhibition effect of PMNFs on sodium dextran sulfate (DSS)-induced colitis was explored. UC was effectively inhibited by PMNFs in this work. PMNFs significantly reduced disease activity index (DAI) score, including weight loss, colon shorten and histopathological abnormalities. The possible mechanism of PMNFs-attenuated colitis was investigated. The results showed that PMNFs reversed DSS-induced oxidative damage, and the antioxidant pathway Nrf2-keap1 signal was activated by PMNFs. Moreover, PMNFs suppressed the expression of pro-inflammatory factors including IL-1β, TNF-α, IFN-β and IL-6 via the inactivation of TLR4/NF-κB pathway in DSS-induced colitis and LPS-treated macrophage. Furthermore, PMNFs treatment prevented the reduction of tight junction proteins (ZO-1, occludin, and claudin-1) and mucin-2 (MUC-2) as well as the up-regulation of epithelial apoptosis caused by DSS. These findings demonstrate that the PMNFs against DSS-induced colitis due to its prevention on oxidative damage, inflammation, and intestine barrier breakdown. Thus, PMNFs have a potential application in the treatment of various oxidative stress or inflammation-related diseases.

## 1. Introduction

Ulcerative colitis (UC) is a chronic, non-specific inflammation of the colon [1]. Patients with UC generally present with symptoms such as abdominal pain, bloody stool, weight loss and enterorrhea [2]. And, high risk of colon cancer is occurred if UC is not treated in a timely manner. Up to now, due to the high incidence of UC, it has become one of the widespread global concern [2]. The pathogenesis of UC is not clearly understood, it has demonstrated that multifactorial pathogenesis are involved in the occurrence and development of UC, such as inflammation, intestinal mucosal barrier injury, environmental factors, genetic predisposition, even the gut microbiota [3].

Present studies demonstrate the mechanism of UC progression include oxidative damage, inflammation and dysfunction of epithelial barrier [4]. It has reported that the increased production of reactive oxygen species (ROS) is an important mechanism of UC development

*Abbreviations:* UC, Ulcerative colitis; IBD, inflammatory bowel disease; ROS, reactive oxygen species; TMCs, two-dimensional transition metal chalcogenide; GPx, glutathione peroxidase; SOD, superoxide dismutase; CAT, catalase; DSS, sodium dextran sulfate; DAI, disease activity index; MPO, **myeloperoxidase**; MDA, malonydialdehyde; NQO1, NADPH quinine oxidoreductase 1; HO-1, heme oxygenase 1; TLR4, Toll-like receptor 4; NF-κB, nuclear factor-kappaB; MUC-2, Mucin-2; TJ, tight junction.

* Corresponding author.
*E-mail address:* xianxiangwang@hotmail.com (X. Wang).
[1] These authors contributed equally to this work.

https://doi.org/10.1016/j.redox.2022.102441
Received 16 June 2022; Received in revised form 6 August 2022; Accepted 11 August 2022
Available online 14 August 2022

[5]. Excessive ROS accumulation can induce protein denaturation, lipid peroxidation, DNA damage, apoptosis, ferroptosis and pyroptosis in intestinal tissues [6]. Growing evidence indicates that antioxidative therapies are useful in the treatment of UC [7]. Besides, some researches highlight that impaired intestinal barrier function is one of the key etiological factors of UC, intestinal barrier dysfunction and destruction are hallmarks of UC, and the breakdown of this barrier is closely associated with the onset and progression of this disease [4]. Therefore, restoring mucosal barrier integrity holds promise as a future treatment approach for UC. Chronic, non-specific inflammation of the colon is also an important reason for UC. Reports showed that NF-κB was activated by LPS-TLR4 pathway and played a critical role in IBD patients as well as experimental colitis models [8].

There are no specific drugs for the UC. Slowing its progression, relieving its symptoms, reducing recurrence rates and preventing the appearance of complications are the principles in the treatment of UC [3]. At present, immunosuppressants, steroid, 5-ASA drugs, biological preparations and adjuvant traditional Chinese medicine are used for the treatment of UC [9,10]. Due to the limited efficacy of these drugs, the potential risk of causing serious side effects and the drug resistance is also a challenge for the therapy of UC, there is an urgent need for effective, available and novel method of treating UC with little side effects. Recently, one therapeutic strategy is to use nanozyme with excellent antioxidant properties to replace conventional drugs to treat inflammation. Nanozyme are a new catalytic nanomaterials with natural enzyme-like characteristics [11]. And, the stability and efficiency of nanozyme make it tend to replace natural enzymes in many applications [12], and it can intervene and regulate the biocatalytic process in vivo by exerting natural enzyme like activity, which is used for the diagnosis and prevention of many diseases [13]. Compared with traditional antioxidant therapeutic drugs, such as small organic molecules, vitamin derivatives and acetylcysteine, the structural stability of nanozyme is better, less affected by the surrounding environment, and the persistence of free radical scavenging activity under physiological conditions is higher. Non-specific damage to proteins, lipids, and nucleic acids caused by ROS is the basic mechanism of several diseases, such as inflammatory and aging-related diseases. Nanozyme with catalase-like activity or superoxide dismutase-like activity can effectively scavenge ROS, thus could prevent or treat ROS-related disease [14].

Transition metal halides (TMHs) nano flakes, especially molybdenum (Mo) nanoparticles, are two-dimensional (2D) materials similar to graphene. Due to its unique physical and chemical properties, so they have been widely studied in recent years in the fields of catalysis, functional electronics, solid lubrication, photovoltaics, energy materials, and more recently biomedical applications. These 2D nanomaterials and their derivatives have atomic thickness and can react with ROS and even remove ROS in the dark. In general, the biocompatibility of 2D materials is the surface functionalization of nanosheets by surfactants, macromolecules, organic solvents, and polymers to improve the stability and biocompatibility of nanosheets under physiological conditions. These materials have good biocompatibility and biosafety, and have great application potential in the field of antioxidant and ROS detection and diagnosis. They can also produce ROS under light and can be used in antibacterial, photodynamic therapy and other biomedical fields [15]. Although TMHs nano flakes have been applied in biomedical field, their application in ROS related diseases is rarely reported. In particular, the potential of transition metal Mo based nanosheets combined with Se in halogens for the treatment of UC has not been confirmed. Therefore, it is of great scientific significance to study the internal therapeutic effect of Mo nanozymes on UC through a variety of therapeutic mechanisms.

Here, a new polyethylene glycol modified $Mo_3Se_4$ nano flakes (PMNFs) was synthesized, and its protective effect on dextran sodium sulfate (DSS)-induced colitis was explored. According to the experimental results, it can be concluded that PMNFs nanozyme have the protective effect on DSS-induced colitis due to its regulatory effects on oxidative damage, inflammation and intestinal barrier. Our study provides evidence for the concept of PMNFs as a safe and potentially effective nano drug for UC.

## 2. Materials and methods

### 2.1. Chemicals and antibodies

Sodium selenite ($Na_2SeO_3$) and polyethylene glycol 6000 were purchased from Chengdu Cologne Chemical Co., Ltd., ammonium molybdate ($(NH_4)_2MoO_4$) were purchased from Tianjin No. 4 Chemical Reagent Factory, glutathione was purchased from Qingdao high tech Industrial Park Haibo Biotechnology Co., Ltd., DSS purchased from Shanghai Sangon Bioengineering Co., Ltd., LPS (L2880, from *Escherichia coli* O55:B5) was purchased from Sigma.

The following antibodies were used in this study: monoclonal rabbit anti-TLR4 (14358S, Cell Signaling Technology), monoclonal rabbit anti–NF–κB p65 (8242, Cell Signaling Technology), monoclonal rabbit anti-p–NF–κB (Ser536) (3033T, Cell Signaling Technology), monoclonal rabbit anti-IκBα (4814, Cell Signaling Technology), monoclonal mouse anti-β-Actin (3700, Cell Signaling Technology), polyclonal rabbit anti-Nrf2 (ab137550, Abcam), monoclonal rabbit anti-Keap1 (8047S, Cell Signaling Technology), polyclonal rabbit anti-NQO1 (ET1702-50, Huabio), polyclonal rabbit anti–HO–1 (ab68477, Abcam), monoclonal mouse anti-claudin-1 (sc-166338, Santa Cruz Biotechnology), monoclonal mouse anti-MUC-2 (sc-7314, Santa Cruz Biotechnology), polyclonal rabbit anti-occludin (27260-1-AP, Proteintech), polyclonal rabbit anti-ZO-1 (21773-1-AP, Proteintech).

### 2.2. Synthesis of PMNFs

PMNFs nanozyme were synthesized by simple hydrothermal method: 0.50 g $Na_2SeO_3$, 0.25 g $(NH4)_2MoO_4$, 1.25 g polyethylene glycol 6000 and 1 g glutathione were dissolved in 20 mL deionized water and stirred, until a transparent solution is formed. The mixture was then transferred to a Teflon lined stainless steel autoclave and heated to 180 °C for 12 h. And then, removed the red-brown liquid product, added 20 mL of absolute ethanol, centrifuged 3 times for 5 min at 4200 rpm, and then filtered the solution with a 0.22 μm filter to remove impurities. Finally, the filtrate was dialyzed with a 500 MWCO dialysis membrane for 12 h and set aside for later use.

### 2.3. Detection of PMNFs characterization

The characterization parameters of PMNFs (morphology, sizes, etc.) were obtained by scanning electron microscope (SEM, JEOL-2100F, Japan). XPS spectra were measured by ESCALAB 250Xi photoelectron spectrometer (Thermo Scientific, USA) to understand elemental composition. FTIR spectrum was obtained by a Fourier transform infrared spectrometer (FTIR-8400S, Shimadzu, Japan) to identify functional groups. The crystal structure of the product was characterized by X-ray diffraction (XRD, DX-2700, Dandong, China). Fluorescence spectrophotometer (Hitachi, F-4500, Tokyo, Japan) and UV–Vis spectrophotometer (Aoyi instrument Co. Ltd., A390, shanghai, China) were used to measure fluorescence and UV–Vis spectra of the systems in this work, respectively.

### 2.4. $H_2O_2$ scavenging activity of PMNFs

The scavenging activity of PMNFs nanozyme against $H_2O_2$ was determined by terephthalic acid (TA) method [16]. The presence of $H_2O_2$ hydroxylated TA at C2 to produce fluorescent 2-hydroxyterephthalic acid (TAOH). In the presence of PMNFs, the fluorescence intensity of TAOH at 450 nm decreased significantly, indicating that $H_2O_2$ was effectively removed by the nanozymes. The specific operation steps are as follows: 150 μL $H_2O_2$ (10 mM) and 150 μL of PMNFs nanozymes

(30–200 μg/mol), add 2.6 mL of PBS buffer (pH = 7.4) and mix in the dark for 4 h. The resulting solution was mixed with 50 μL $FeSO_4$ (1 mM) for 1 h, then added to 50 μL 0.1 M NaOH terephthalic acid (TA, 30 mM). After 60 min, fluorescence emission was measured by fluorescence spectrometer.

### 2.5. •OH scavenging activity of PMNFs

The hydroxyl radical (•OH) scavenging activity of PMNFs was also determined by TA method. In the presence of PMNFs nanozymes, the fluorescence of TAOH decreased significantly, indicating that PMNFs nanozymes effectively scavenged hydroxyl radicals generated by Fenton reaction. The specific operation steps are as follows: 100 μL $H_2O_2$ (10 mM) and 100 μL $FeSO_4$ (1 mM) was mixed for 30 min to form hydroxyl radical. 100 μL PMNFs nanozymes (30–200 μg/mol) were added to the hydroxyl radical solution 50 μL (3 mM), oscillate at 40 °C for 1 h. 50 μL TA (30 mM, 0.1 M NaOH) and 2.8 mL of PBS buffer (pH = 7.4) was added to the mixture and oscillated for 1 h. After the PMNFs is removed by centrifugation, the fluorescence emission of the solution is measured by fluorescence spectrometer.

### 2.6. $O_2^-$ scavenging activity of PMNFs

Xanthine (XAN) and xanthine oxidase (XOD) systems were selected to evaluate the superoxide anion ($O_2^-$) scavenging activity [17]. In a specific example, mix 50 μL XAN (5 mM) 100 μL, PMNFs (0–200 μM) and 100 μL azoblue tetrazole, then add 50 μL XOD (0.5 U $mL^{-1}$). The mixture was shaken at 25 °C for 1 h and centrifuged at 4000 rpm for 5 min. PMNFs was removed from the solution and its absorbance was measured at 560 nm.

### 2.7. DPPH radical scavenging activity of PMNFs

DPPH (2,2-diphenyl-1-picric acid hydrazine) is a dark crystal powder composed of stable free radical molecules for the determination of antioxidants [18,19]. The free radical scavenging activity value is expressed as the ratio of the percentage decrease in absorbance of the sample at 517 nm to the absorbance of DPPH solution without extract. Simply put, first dissolve 0.4 g DPPH powder in 20 ml absolute ethanol to prepare 0.2 mg/ml DPPH solution. A series of sample solutions with different concentrations were prepared and mixed with DPPH solution. After dark for 30 min at room temperature, the absorbance value was detected at 517 nm by multifunctional fluorescence chemiluminescence immunoanalyzer. The free radical scavenging capacity of antioxidants is calculated by the following formula:

$$\text{scavenging rate } (\%) = [(A_c - A_s)/A_c] * 100\%$$

*Ac* is control absorbance and *As* is sample absorbance.

Calculation of half clearance: the free radical scavenging capacity of antioxidants is expressed by the half clearance of DPPH ($IC_{50}$ value). Prepare the sample solution into solutions with different concentrations, measure the DPPH radical scavenging rate, draw the concentration curve of the solution to be tested for DPPH radical scavenging rate, and when the DPPH radical scavenging rate is 50%, read the curve or calculate the required sample solution concentration, i.e. $IC_{50}$ value.

### 2.8. CAT-like activity of PMNFs

Fluorescence spectroscopy was used to study the catalase-like activity of PMNFs nanozymes. $H_2O_2$ can be decomposed into •OH, which will react with TA to generate a fluorescent substance TAOH with excitation/emission peaks at 315/425 nm [20,21], respectively. In the presence of catalase (CAT), $H_2O_2$ is decomposed into $H_2O$ and $O_2$ cannot produce the fluorescent substance TAOH. Therefore, by monitoring the fluorescence signal in the solution system, the elimination of $H_2O_2$ can be studied. Briefly, the specific operation steps are as follows: 150 μL $H_2O_2$ (10 mM) and 150 μL PMNFs nanozymes (30–300 μg/mol), add 2.6 mL PBS buffer (pH = 7.4), and mix in the dark for 4 h. The resulting solution was mixed with 50 μL $FeSO_4$ (1 mM) for 1 h, then added 50 μL of 0.1 M NaOH terephthalic acid (TA, 30 mM). After 60 min, fluorescence emission was measured by fluorescence spectrometer.

### 2.9. Peroxidase-like activity of PMNFs

The peroxidase-like activity and steady-state kinetics of PMNFs nanozyme were studied by using 3,3 ′, 5,5' – tetramethylbenzidine (TMB) and $H_2O_2$ as reaction models [22,23]. In short, TMB (5 mM) 100 μL, $H_2O_2$ (100 mM) 100 μL and PMNFs nanozymes 100 μL heat at 25 °C for 10 min. The volume of the reaction system was adjusted to 3 ml using 0.1 M acetic acid buffer (pH = 3). In the mixed system, the absorbance of TMB oxidation products increased with the increase of PMNFs concentration. The formation of the complex was detected by UV/Vis, and the absorbance change at 652 nm was recorded. Investigate the effects of pH, temperature on peroxidase-like activity and study steady-state kinetics under optimal conditions.

Line weaver burk double reciprocal curve obtained by varying $H_2O_2$ or TMB concentration for determination of enzyme affinity. The affinity of the enzyme to the substrate can be evaluated by the determination of Michaelis gate constant ($K_m$). Use the following relationship:

$$\frac{1}{V} = (K_m / Vmax)(1 / [S]) + 1 \Big/ Vmax$$

where V is the initial catalytic rate, $V_{max}$ is the maximum rate conversion, which is obtained when the catalytic sites on the enzyme are saturated with substrate concentration. [S] is the concentration of substrate and $K_m$ is the Michaelis constant. Maximum initial velocity ($V_{max}$) and Michaelis–Menten constant ($K_m$) were obtained using Lineweaver–Burk plots.

### 2.10. GPx-like activity of PMNFs

Glutathione (GSH) reacts with 5,5 ′-dithiondinitrobenzoic acid (DTNB) to form a compound with 412 nm characteristic absorption [20]. During the test, glutathione is oxidized to oxidized glutathione (GSSG). The glutathione peroxidase (GPx) activity of PMNFs was measured by DTNB direct method. The decrease of GSH concentration was directly proportional to the catalytic activity of PMNFs.

### 2.11. SOD-like activity of PMNFs

In order to evaluate the superoxide scavenging activity, the xanthine (XAN) and xanthine oxidase (XOD) systems were selected for evaluation. Xanthine oxidase (XO) oxidizes xanthine to generate $O_2^-$, which can reduce the nitroblue tetrazole to blue methylhydrazone, and substances with SOD activity can eliminate $O_2^-$, thereby inhibiting the formation of methylhydrazone. Its absorbance at 560 nm was measured with a UV–Vis spectrophotometer. In a specific example, mix 50 μL XAN (5 mM), 100 μL PMNFs nanozymes (0–200 μM), and 100 μL nitroblue tetrazole, and then add 50 μL XOD (0.5 U $mL^{-1}$). The mixture was shaken at 25 °C for 1 h, and centrifuged at 4000 rpm for 5 min. Remove PMNFs from the solution, and then measure the absorbance at 560 nm.

### 2.12. Animal experiments

Male ICR mice (6 weeks) were obtained from Dashuo Biological Technology (Chengdu, China). All mice were fed with the standard pellet diet with free access to water, and raised in individual cages in standard environment (light/dark cycle, 12 h/12 h; temperature, 25 ± 2 °C). After 7-day acclimatization, the animals were randomly classified into four groups (18 mice in each group). Each animal procedure was

carried out following guidelines of Animal Care and the Ethics Committee of Sichuan Agricultural University (Approval No:2012-024, Chengdu, China). For induction of DSS-induced colitis and treatment studies, experimental colitis was induced by adding DSS (3% wt/vol) to the drinking water for 9 days. Mice were treated with PMNFs (100 mg/kg) or the same volume of PBS once a day with oral gavage. Mice were weighed daily and monitored for clinical signs of colitis. A colitis disease activity index (DAI) was calculated for each mouse daily based on the following criteria [24]: weight loss from baseline (0, no weight loss; 1, 1–3% weight loss; 2, 3–6% weight loss; 3, 6–9% weight loss; 4, >9% weight loss); stool consistency (0, normal; 2, loose stool; 4, diarrhea), and fecal blood (0, none; 2, blood visible in stool; 4, gross bleeding). Gross bleeding was defined as fresh perianal blood with obvious hematochezia. On day 10, all mice were anesthetized for whole blood collection. Afterwards, the colon was removed, measured for its length, and stored at −80 °C for subsequent analysis.

### 2.13. Cell culture

The RAW264.7 macrophages were cultured within the DMEM (Gibco BRL, Grand Island, NY) that contained the 10% fetal bovine serum (FBS, heat-inactivated) and penicillin-streptomycin antibiotics (both 50 μg/ml), followed by incubation within the incubator under 37 °C and 5% $CO_2$ conditions. For induction of LPS-induced inflammation and treatment studies, RAW264.7 cells were primed with 1 μg/ml of LPS for 6 h followed by treatment with or without 1 mg/ml PMNFs (4 h).

### 2.14. Pathological observations of colon

On day 10 of the experiment, mice were executed for collecting colon samples. Afterwards, samples were fixed in 4% paraformaldehyde fixation, dehydrated with alcohol, embedded in paraffin. Then, these samples were cut into slices (with a thickness of 4 μm) and dyed by hematoxylin and eosin (H&E). The histopathological features evaluated covered [24]: acute and/or chronic inflammation, hyperplastic changes of the colon epithelium, and crypt distortion or damage, fibrosis, and neoplasia. Three independent parameters were measured: inflammatory cell infiltrate, extent of hyperplasia, and crypt damage. The total histological score was calculated by summing of the three independent scores with a maximum score of 12. Inflammation was assessed using a scoring system from the literature: 0 is no inflammation; 1 is mild chronic mucosal inflammation; 2 is mild acute or moderate chronic mucosal and submucosal inflammation; 3is severe acute or chronic mucosal, submucosal, and transmural inflammation. Hyperplastic changes were scored as the increase in epithelial cell numbers in crypts relative to baseline epithelial numbers per crypt as follows: 0 is none or minimal (<20%); 1 is mild (21–35%); 2 is moderate (36–50%); 3 is marked (>50%). Crypt damage was scored as: 0 is none; 1 is only surface epithelium damaged; 2 is surface crypt and epithelium damaged; 3 is entire crypt lost and surface epithelium damaged; 4 is entire crypt and epithelium lost.

### 2.15. Myeloperoxidase (MPO) in colon tissue

The colons were homogenized and the supernatants were partially isolated to determine the protein concentration of the colon using the BCA protein assay kit (CWBIO, Beijing, China). Remaining supernatant were used to measure the levels of myeloperoxidase (MPO) according to manufacturer's instructions of MPO assay kit (Nanjing Jiancheng Bioengineering Institute, Nanjing, China).

### 2.16. Oxidative stress analysis

Colon samples were washed within chilled saline solution, weighed and homogenized with nine volumes of ice-cold 0.9% NaCl solution, followed by centrifugation at 3500 rpm for 10 min at 4 °C. By inserting the supernatant to new eppendorf tubes, the activity of T-AOC (Cat. No. A015), SOD (Cat. No. A001-1), CAT (Cat. No. A007-1), GPx (Cat. No. A005), GSH (Cat. No. A061-1), as well as MDA (Cat. No. A003-1) were investigated using the commercially available kits (Nanjing Jiancheng Bioengineering Institute, Nanjing, China) in accordance with the specifications.

### 2.17. Measurements of intracellular ROS

The ROS contents were measured using DCFH-DA (M36008, Invitrogen). The ROS in the colon was measured by DCFH-DA staining in the colon frozen section. The colon section was incubated with 20 μM DCFH-DA for 20 min. Then all images were acquired with a fluorescence microscope.

RAW264.7 cells plated on 96-well plate for 24 h. RAW264.7 cells were primed with 1 μg/ml of LPS for 6 h followed by treatment with or without 1 mg/ml PMNFs for 4 h. After washing by PBS twice, cells were incubated with 20 μM DCFH-DA for 20 min. Then, cells were rinsed by PBS twice, and the Synergy 2 multimode plate reader (BioTek Instruments) was used to determine fluorescence intensity.

RAW264.7 cells plated on coverslips for 24 h. After treated with LPS and PMNFs, cells were incubated with 20 μM DCFH-DA for 20 min. Then, cells were rinsed by PBS twice and fixed with 4% paraformaldehyde. All images were acquired with a fluorescence microscope.

### 2.18. Immunofluorescence

RAW264.7 cells plated on coverslips for 24 h. After treated with LPS and PMNFs, cells were fixed with 4% paraformaldehyde. After fixation, cells were permeabilized with 0.2% Triton X-100 for 5 min and blocked with 10% goat serum (G9032, Sigma) for 2 h at room temperature. Cells were incubated with NF-κB p65, followed by Alexa Fluor 488-conjugated anti-rabbit IgG secondary antibody. The nuclei of cells were stained with DAPI. All images were acquired with a fluorescence microscope. The percentage of cells with NF-kB nuclear translocation was quantified.

### 2.19. Immunohistochemistry

For immunohistochemistry staining [25], tissue slides were deparaffinized in xylene and rehydrated in alcohol. Endogenous peroxidase was blocked with 3% hydrogen peroxide. Antigen retrieval was performed by incubating the sections in boiling 10 mM sodium citrate pH 6.0 followed by incubation with the indicated primary antibody overnight at 4 °C. The slices washed with PBS were allowed to expose to 1% biotinylated secondary antibody goat anti-rabbit IgG (Boster, Wuhan, China) at 37 °C for 1 h, followed by incubation with strept avidin-biotin complex (SABC) (Boster, Wuhan, China) at 37 °C for 30 min. For visualizing immunoreaction, diaminobenzidine hydrochlo-ride (DAB) (Boster, Wuhan, China) was used to immerse the slices. Immediately after a brown color staining was visualized, the slices were observed under a microscope and stopped through immersion in distilled water. Sections were then counterstained with hematoxylin. For negative controls, the primary antibody was excluded. For evaluation and scoring of immunohistochemical data, 10 fields were randomly selected under high power magnification (40×) for evaluation. The quantitative analysis of the average optical density of Immunohistochemistry staining was performed using Image-Pro Plus software 6.0 (Media Cybernetics, USA).

### 2.20. Western blot analysis

Tissues and cells to be lysed in the pre-chilled RIPA buffer. 12% SDS-PAGE was made for separating proteins, with subsequent transfer to PVDF membranes. Afterwards, 5% non-fat milk dissolved in TBST was

employed for blocking membranes, followed by incubation by using primary antibodies as well as HRP-labeled secondary antibodies successively. The ECL detection kit (GE Healthcare, Piscataway, NJ, USA) was used in visualization. The protein bands could be visualized with Bio-Rad ChemiDoc XRS + System (Bio-Rad Laboratories, Inc., Hercules, CA, USA). ImageJ2x software had been adopted for determining the significant difference in protein expression.

### 2.21. Enzyme-linked immunosorbent assay

Mouse cytokines in serum, culture supernatants and the colon extracts were measured with ELISA kits (Tongwei, China) for IL-1β (TW15343), IL-6 (TW11676), TNF-α (TW8111), and IFN-β (TW8368), according to the manufacturer's directions.

### 2.22. RNA extraction and quantitative real-time PCR (qRT-PCR)

RNAiso Plus (9109; Takara, China) was chosen in total RNA extraction according to the manufacturer's protocol. cDNA was synthesized by the Prim-Script™ RT reagent Kit (RR047A, Takara, China) in accordance with corresponding specifications. The gene data came from National Center for Biotechnology Information (NCBI), and Sangon (Shanghai, China) took charge of primer design and synthesis. The primer sequences were showed in Table 1. The qRT-PCR was performed using SYBR® Premix Ex TaqTMII (RR820A, Takara, China) according to corresponding specifications. All the reactions needed to be performed at 95 °C for 10 min, and then at 95 °C for 10 min, at 60 °C for 20 s, and at 72 °C for 20 s. Subsequently, melt curves were investigated to identify PCR specificity. Additionally, the results of qRT-PCR were analyzed using the $2^{-\Delta\Delta CT}$ method.

### 2.23. PAS staining

PAS stain kits were purchased from solarbio life sciences (G1285). Briefly, paraffin-embedded sections were dewaxed in xylene, rehydrated in ethanol, and rinsed in distilled water. After oxidation in periodic acid for 15 min, each section was stained with Schiff reagent for 10 min, rinsed with distilled water for 5 min, and counterstained with hematoxylin for 2 min. The sections were subsequently washed, dehydrated, and sealed with a neutral resin for microscopic examination.

### 2.24. Apoptosis detection

TUNEL assay was conducted to detect apoptosis, and nuclear DNA fragmentation during apoptosis in situ was detected with the apoptosis detection kit (C1091, Beyotime Biotechnology). According to the method of reference [25]. Briefly, colon sections (4 μm thick) were rehydrated in a series of xylene and ethanol solutions and then rinsed in ddH2O, digested with 50 μL proteinase K for 15 min, and incubated with 3% $H_2O_2$ in methanol for 15 min at room temperature to inactivate endogenous peroxidase. The sections were transferred to a reaction mixture containing biotin-dUTP terminal deoxynucleotidyl and incubated in a humidified chamber for 1 h at 37 °C, followed by washing in PBS, pH 7.2–7.4. Sections were incubated in Converter-POD (HRP) for 30 min at 37 °C. Reaction product was visualized with DAB kit (AR1022, Boster, Wuhan, China). After final washing in dd$H_2O$, slices were lightly counterstained with hematoxylin, dehydrated in ethanol, cleared in xylene and mounted. The nuclei of apoptotic cells containing DNA strand breaks were stained brown. Data were presented in a form of mean TUNEL-positive cell count/crypt.

### 2.25. Statistical analysis

The results had been illustrated by mean ± SD. One-way or two-way ANOVA was chosen for comparing significant differences between control group and experimental group with SPSS17.0. $P < 0.05$ suggested the value was statistically significant.

## 3. Results

### 3.1. Synthesis of PMNFs and characterization of PMNFs

PMNFs were prepared by one pot hydrothermal method (Fig. 1a). The morphological characteristics were observed by scanning electron microscope (SEM). As shown in Fig. 1b, the morphology of PMNFs nanozyme were in the form of sheets with obvious aggregation distribution, and, the transverse particle size is between 0.4 and 2 μm. The X-ray diffraction (XRD) spectrum shows the diffraction mode of $Mo_3Se_4$ crystal (Fig. S3). The characterization peak of PMNFs nanozyme was 12.87°, 26.89°, 29.81°, 33.76°, 37.71°, and it belong to hexagonal 2H phase $Mo_3Se_4$ according to the standard card (JCPDS No. 21–0575), they should correspond to the crystal planes (001), (002), (111), (102) and

**Table 1**
Primer sequences of genes selected for analysis by qRT-PCR.

| Target gene | Accession number | Primer | Primer sequence (5′–3′) | Product size | Tm (°C) |
|---|---|---|---|---|---|
| CuZn-SOD | NM_011434 | Forward | GGGTTCCACGTCCATCAGTA | 113bp | 60 |
| | | Reverse | CAGGTCTCCAACATGCCTCT | | |
| Mn-SOD | NM_013671 | Forward | AACTCAGGTCGCTCTTCAGC | 113bp | 60 |
| | | Reverse | CTCCAGCAACTCTCCTTTGG | | |
| CAT | NM-009804 | Forward | CCTATTGCCGTTCGATTCTC | 119bp | 59 |
| | | Reverse | CCCACAAGATCCCAGTTACC | | |
| GPx | NM_008160 | Forward | TACACCGAGATGAACGATCTG | 102bp | 57 |
| | | Reverse | ATTCTTGCCATTCTCCTGGT | | |
| TNF-a | NM_204267 | Forward | CCCCTACCCTGTCCCACAA | 100bp | 58 |
| | | Reverse | TGAGTACTGCGGAGGGTTCAT | | |
| INF-β | NM_010510.1 | Forward | CGTGGGAGATGTCCTCAACT | 122bp | 58 |
| | | Reverse | CCTGAAGATCTCTGCTCGGAC | | |
| IL-1β | NM_008361 | Forward | AATGCCACCTTTTGACAGTGAT | 132bp | 61 |
| | | Reverse | TGCTGCGAGATTTGAAGCTG | | |
| IL-6 | NM_001314054.1 | Forward | ACAAAGCCAGAGTCCTTCAGAG | 86bp | 60 |
| | | Reverse | GCCACTCCTTCTGTGACTCC | | |
| claudin-1 | NM_016674.4 | Forward | CCCTTCAGCAGAGCAAGGTT | 123 bp | 60 |
| | | Reverse | TAGGGCAACCAAGTGCCTTT | | |
| occludin | NM_008756.2 | Forward | TAGTGGCTTTGGCTACGGAGGT | 99bp | 60 |
| | | Reverse | AGGAAGCCTTTGGCTGCTCTTG | | |
| ZO-1 | NM_009386.2 | Forward | GAGCCCCCTAGTGATGTGTG | 80 bp | 60 |
| | | Reverse | TAGGGTCACAGTGTGGCAAG | | |
| β-actin | NM_007393 | Forward | GCTGTGCTATGTTGCTCTAG | 117bp | 60 |
| | | Reverse | CGCTCGTTGCCAATAGTG | | |

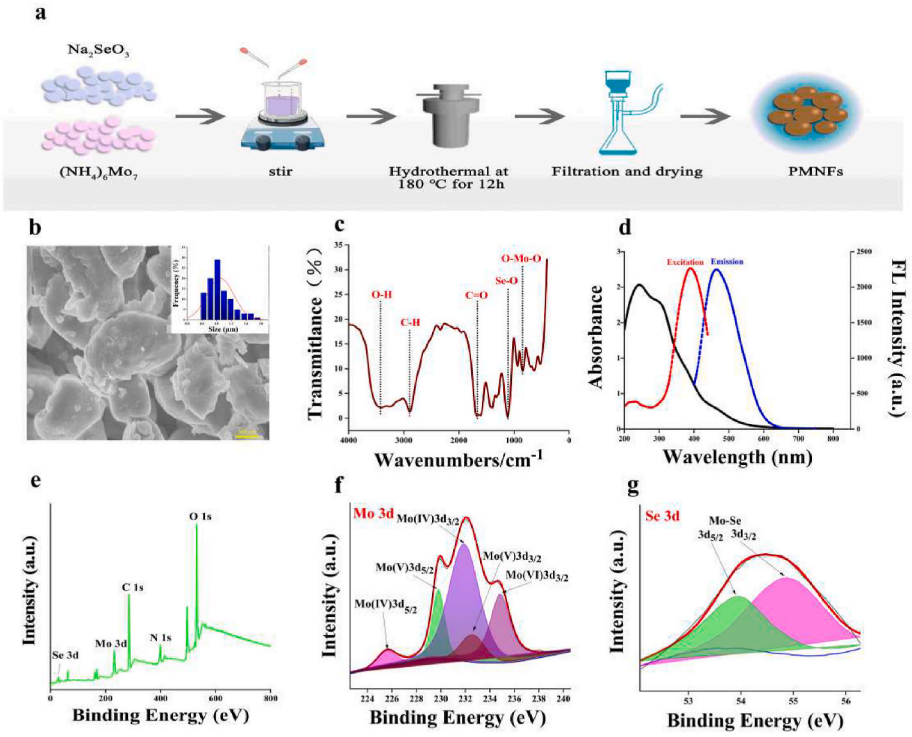


**Fig. 1.** Synthesis of PMNFs and characterization of PMNFs. (a) Schematic diagram of the preparation of PMNFs. (b) SEM image and the size of PMNFs. (c) FT-IR spectrum of PMNFs. (d) UV–Vis absorption, fluorescence excitation and emission spectra of PMNFs. (e) XPS general scan. (f) Core level spectra of Mo 3d. (g) Core level spectra of Se 3d.

(020), respectively. By Fourier infrared spectroscopy (FTIR), the molecular structure and functional groups of PMNFs were characterized. As shown in Fig. 1c, O–Mo–O and Se–O bonds corresponded to the stretching vibrations at 839 $cm^{-1}$ and 1109 $cm^{-1}$ respectively, while the stretching vibrations at 1672 $cm^{-1}$, 2892 $cm^{-1}$ and 3400 $cm^{-1}$ may come from C═O, C–H and O–H bonds respectively. The typical peaks of vibration showed that PEG successfully modified $Mo_3Se_4$ [17,22]. PEG modification could prevent the agglomeration of nano sheets and increase its biocompatibility and water solubility. XPS spectra in Fig. 1e reveal the elemental and chemical composition of PMNFs. It can be found that C, O, N, Mo and Se are the main elements of PMNFs. In the core XPS spectrum of Mo (3D) as shown in Fig. 1f, there were four peaks of 225.6 eV, 231.9 eV, 229.8 eV and 232.9 eV, which belonged to $3d_{5/2}$ and $3d_{3/2}$ of Mo (IV) as well as $3d_{5/2}$ and $3d_{3/2}$ of Mo (V), respectively. The XPS peak of Mo (VI) ($3d_{3/2}$) in high oxidation state at 234.9 eV represented the formation probability of $MoO_3$ [26]. In the XPS spectrum of Se 3D (Fig. 1g), it also can be observed that the characteristic peaks [27,28] of Mo–Se bond exist at 54.9 eV and 53.9 eV, corresponding to Se $3d_{3/2}$ and Se $3d_{5/2}$, respectively. In the C 1s spectrum (Fig. S1a), C═C, C–C and C═O bonds can be confirmed by the three peaks of 284.4 eV, 285.8 eV and 288.2 eV, respectively. The O 1s peaks of 531.8 eV and 535.5 eV respectively belonged to the vibration of C–O–Mo and O–OH bonds (Fig. S1b). There were three peaks in the inverse N 1s spectrum (Fig. S1c), among which the main peak of 399.6 eV come from neutral amine nitrogen, and another two peaks of 401.3 eV and 396.8 eV are assigned to the binding energy of positively charged nitrogen and imine nitrogen, respectively [29].

The optical properties of PMNFs were showed in Fig. 1d. In the absorption spectrum of PMNFs, there was a strong absorption band, ranging from 200 nm to 400 nm, and PMNFs emitted blue fluorescence at 460 nm when it was excited at 380 nm. As the excitation wavelength varies from 350 nm to 430 nm, the fluorescence emission wavelength of PMNFs also varies from 450 nm to 510 nm, which is showed in Fig. S2 indicating the fluorescence excitation dependence of PMNFs.

### 3.2. ROS scavenging activities of PMNFs

Three representative ROS were selected to measure the ability of PMNFs to remove ROS, including $H_2O_2$, $O_2^-$, and •OH. As shown in Fig. 2, ROS scavenging activity of PMNFs enhances with increasing concentration. The $H_2O_2$ scavenging activity of PMNFs nanozymes was measured by terephthalic acid (TA) [16]. The presence of $H_2O_2$ caused TA to be hydroxylated at C2, producing fluorescent 2-hydroxyterephthalic acid (TAOH). In the presence of nanozymes, the fluorescence intensity of TAOH at 450 nm is significantly reduced (Fig. 2e), and about 80% of $H_2O_2$ was decomposed by 200 μg/mL PMNFs (Fig. 2a). The scavenging activity of •OH was evaluated by TA method. In the presence of PMNFs, the fluorescence of TAOH was significantly reduced (Fig. 2f), which mean that PMNFs could effectively remove •OH generated by the Fenton reaction. When treated with 200 μg/mL PMNFs, approximately 70% of •OH radicals were removed (Fig. 2b). More than 90% of $O_2^-$ were decomposed by 150 μg/mL PMNFs treatment (Fig. 2c), corresponding to the spectrogram in Fig. 2g. In order to further confirm the antioxidant properties of PMNFs, a classic 2,2-diphenyl-1-pyridine hydrazide (DPPH) free radical scavenging experiment was used in this study. As shown in Fig. 2d, more than 85% of free radicals were eliminated when treated with 500 μg/mL PMNFs, and half-inhibitory concentration ($IC_{50}$) value is 217.5 μg/mL.

### 3.3. Multienzyme-like activity of PMNFs

The multi-enzyme activities of PMNFs were further investigated. CAT is an indispensable enzyme in the biological antioxidant enzyme system because through its catalysis, excess $H_2O_2$ in the body can be decomposed into $H_2O$ and $O_2$, thereby protecting cells and tissues from oxidative damage. Therefore, we investigated the CAT activity of PMNFs. Using TAOH as a fluorescent probe to investigate the concentration-dependent CAT-like activity of PMNFs (Fig. 2h). With the increase of PMNFs concentration, the scavenging rate of $H_2O_2$ was also

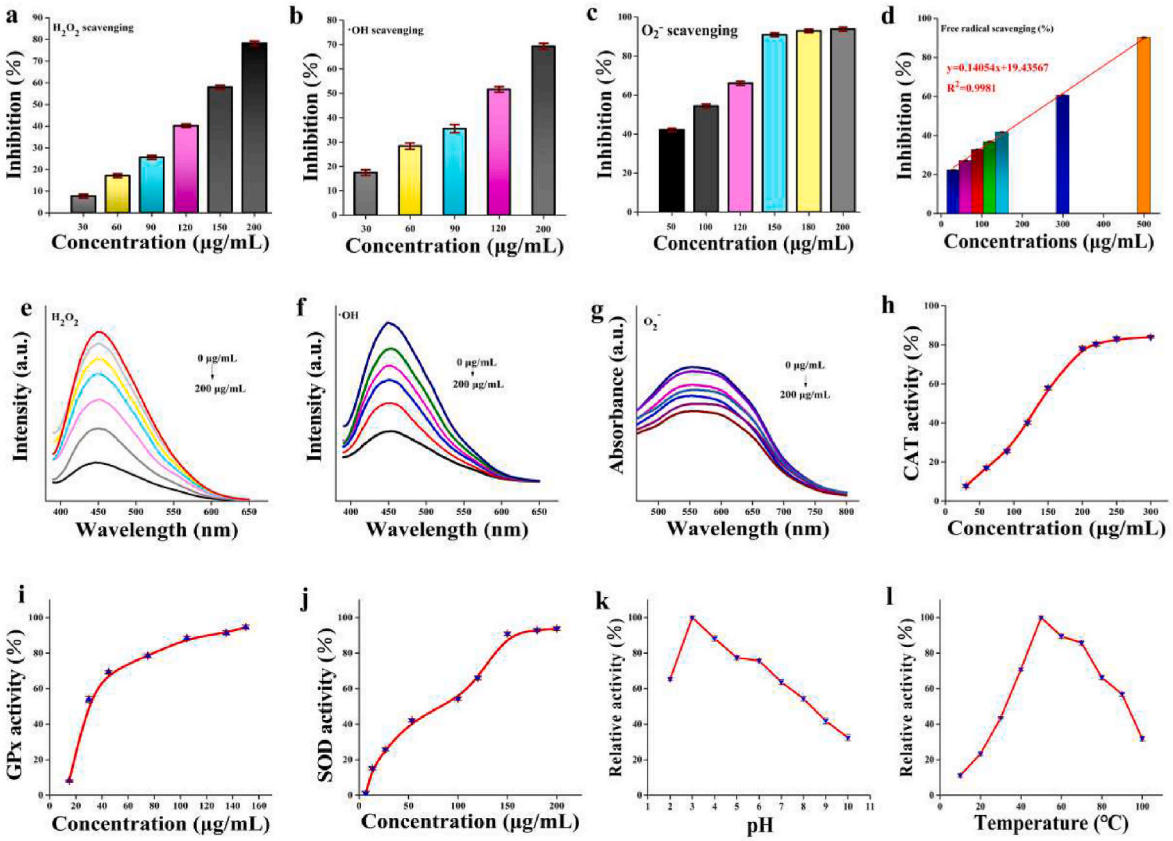


**Fig. 2.** ROS scavenging and multi-enzyme-like antioxidative activity of PMNFs. (a) $H_2O_2$, (b) •OH, (c) $O_2^-$, (d) free radical scavenging ability of PMNFs. (e) $H_2O_2$ radical scavenging fluorescence spectra of PMNFs (from bottom to top: 0, 30, 60, 90, 120, 150, 200 mg/mL), $H_2O_2$ (10 mM) and TA (30 mM), (f) •OH radical scavenging fluorescence spectra of PMNFs (from bottom to top: 0, 30, 60, 90, 120, 200 mg/mL), $H_2O_2$ (10 mM) and TA (30 mM), (g) $O_2^-$ radical scavenging fluorescence spectra of PMNFs (samples containing XAN (5 mM) and XOD (0.5 U mL)$^{-1}$), azoblue tetrazole (0.75 mM) and PMNFs (50–200 mg/mL)), (h) CAT-like, (i) GPx-like, and (j) SOD-like activity of PMNFs. The peroxidase-like activity of the PMNFs at different (k) PH, and (l) temperature conditions.

increased gradually, indicating that PMNFs had good CAT-like catalytic ability. The peroxidase (POD)-like activity of PMNFs was also detected by using 3,3′,5,5′-tetramethylbenzidine (TMB) as the chromogenic substrate. The optimal enzymatic reaction conditions for PMNFs nanozymes was shown in Fig. 2k and l. As shown in Fig. S4, using TMB and $H_2O_2$ as substrates, steady-state kinetic analysis was further performed to evaluate POD activity, the reaction exhibits the typical Michaelis-Menten equation (Mie's equation) kinetics. The affinity between the catalyst and the substrate is expressed as $K_m$, that is, the higher the $K_m$, the weaker the affinity. With TMB as the substrate, the $K_m$ value of the PMNFs was 0.137 mM, and the Vmax value was $18.6 \times 10^{-8}$Ms$^{-1}$. The $K_m$ value of the PMNFs with $H_2O_2$ as the substrate was 8.765 mM, and the $V_{max}$ value was $21.2 \times 10^{-7}$Ms$^{-1}$. Compared with other Ce@$Fe_3O_4$ (6.942 mM) [30], Fe@$CeO_2$ (0.176 mM) [31] nanomaterials and natural enzyme HRP (0.434 mM) [32] used as peroxidase mimics with TMB as substrate (Supplementary Table 1), the $K_m$ of the prepared PMNFs (0.137 mM) is much lower. We also studied the concentration dependence of the SOD-like activity of PMNFs (0–200 μg/mL). As shown in Fig. 2j, it showed that PMNFs have SOD-like activity, and the median effect concentration ($EC_{50}$) of PMNFs was 1.5938 μg/mL, which was almost more than two times than the natural SOD [20]. Generally, GPx generally uses cell body glutathione (GSH) as a reducing agent to catalyze $H_2O_2$ to water to generate oxidized glutathione (GSSG). GSH reacts with 5,5′-dithiodinitrobenzoic acid (DTNB) to produce a compound with a characteristic absorption of 412 nm, as shown in Fig. 2i, by independently changing the 0–150 μg/mL PMNFs concentration, the GPx activity of PMNFs was studied. It was found that as the concentration of PMNFs increased, the UV absorption at 412 nm decreased significantly, indicating that PMNFs have a good concentration-dependent GPx-like activity.

### 3.4. PMNFs alleviates DSS-induced colitis in mice

Here, we investigated whether PMNFs can ameliorate or alleviate intestinal inflammation caused by oral DSS. The mice were divided into two groups, one group was fed DSS only, and the other group was fed PMNFs along with DSS. The amount and method of DSS fed in the two groups were the same, that is, 3% DSS (w/v) was added to their drinking water, and PMNFs (100 mg/kg) was force-fed to the mice once a day. The experiments were carried out for 9 days. The results illustrated those mice in the DSS group showed significant symptoms of DSS-induced colitis, including a significant decrease in weight and colon length, and an increase in disease activity index (DAI) and histopathological scores comparing to the control group. However, the mice co-treated with PMNFs showed less severe symptoms of colitis, i.e. less weight loss ($p < 0.001$) (Fig. 3a), lower DAI scores (Figuer 3b) and less shortening of the colon (Fig. 3c). Meanwhile, after treatment with PMNFs at different concentration (0–400 mg/kg) for 9 days, there are no significantly changes on the body weight (Fig. S5a), hepatic function (Figs. S5b and c) and renal function (Figs. S5d and e), and there were no histopathological lesions in the liver, kidney, spleen, lung and colon (Fig. S5f). And, we also found that DSS-induced changes could be rescued by treatment with different dose of PMNFs (Fig. S6). Myeloperoxidase (MPO), a glycosylase present in neutrophil and monocyte granules, can be acts as a biological marker to assess the disease status of IBD. Therefore, MPO activity can be measured as the severity of neutrophils infiltration. Colonic MPO activity was significantly lower after PMNFs co-treatment (Fig. 3d), indicating PMNFs suppressed the

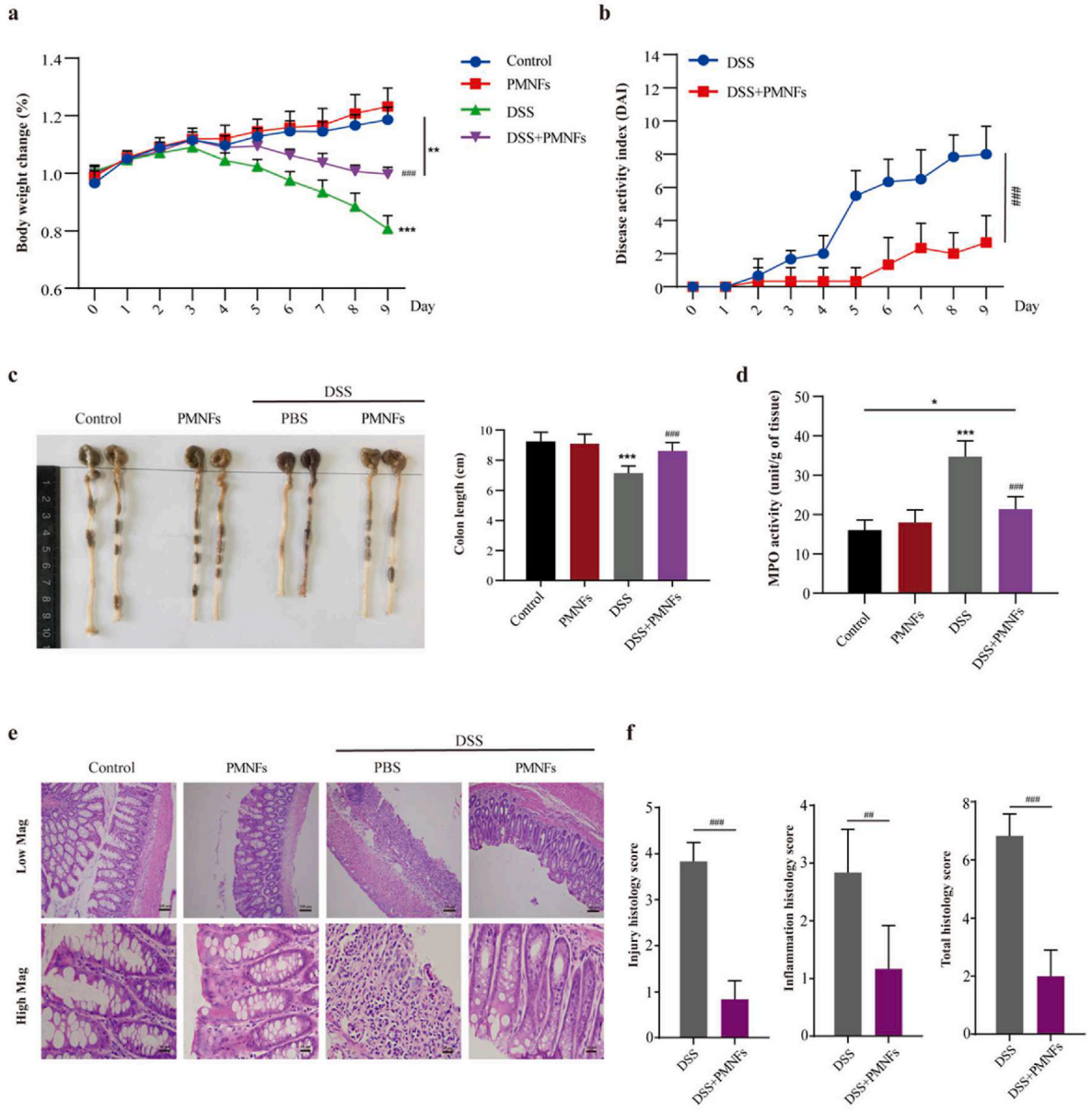


**Fig. 3.** PMNFs suppresses the symptoms of DSS-induced colitis mice model. (a) Daily change of body weight of mice. (b) DAI of colitis. (c) Representative photograph and statistical analysis of colon length on day 10 of the experiment. (d) MPO activities changes. (e) Representative histopathology changes in the colon and histopathology scores. Low Mag: Scale bars, 100 μm. High Mag: Scale bars, 20 μm. (f) The histological score was calculated as described in Methods. H&E-staining. For all quantifications, data (mean ± SD) were from the indicated number of independent experiments and analyzed with two-way ANOVA. *P < 0.05, **P < 0.01, ***P < 0.001 versus the control group; #P < 0.05, ##P < 0.01, ###P < 0.001 versus DSS-induced colitis group.

neutrophil infiltration in the colon. Furthermore, administration of PMNFs significantly attenuated the histological signs of colitis, including tissue injury and inflammatory infiltrates (Fig. 3e and f). These results indicate that PMNFs can efficiently relieve the symptom of DSS-induced colitis. Next, the potential mechanism of PMNFs-attenuated DSS-induced colitis was explored, including oxidative stress, inflammation and intestine barrier.

### 3.5. PMNFs against DSS-induced colitis though inhibiting oxidative stress

Oxidative damage is the basic mechanism of several disease including the UC [5,33]. As shown in Fig. 4a, ROS levels were significantly increased in the colon induced by DSS, PMNFs treatment inhibited the ROS generation. Meanwhile, malonydialdehyde (MDA), an oxidative damage marker, was also significantly decreased by PMNFs in the colon (Fig. 4b). The antioxidant capacity including T-AOC, CAT, GPx and SOD activity and GSH levels were rescued by PMNFs (Fig. 4c). In addition, our results also confirmed that PMNFs could scavenge the ROS induced by LPS in RAW 264.7 macrophages (Figs. S7d and e).

Moreover, the antioxidant pathway Nrf2-keap1 signaling pathway was detected. As shown in Fig. 4d, the increase in keap1 protein levels and decrease in Nrf2 protein level indicated that Nrf2-keap1 signaling pathway was suppressed in DSS-induced colitis mice (Fig. 4d), PMNFs treatment reversed this suppression (Fig. 4d). Meanwhile, the downstream proteins of Nrf2-keap1 signaling pathway were detected, the results showed that NADPH quinone oxidoreductase 1 (NQO1) and heme oxygenase 1 (HO-1) levels were increased after co-treatment with PMNFs (Fig. 4d). And, the mRNA levels of antioxidant enzymes (CuZn-SOD, Mn-SOD, CAT and GPx) were significantly increased by PMNFs co-treatment compared with the DSS group (Fig. 4e). In summary, the anti-oxidative activity of PMNFs should be mediated by directly scavenging ROS and the reconstitution of the Nrf2-mediated cellular anti-oxidative

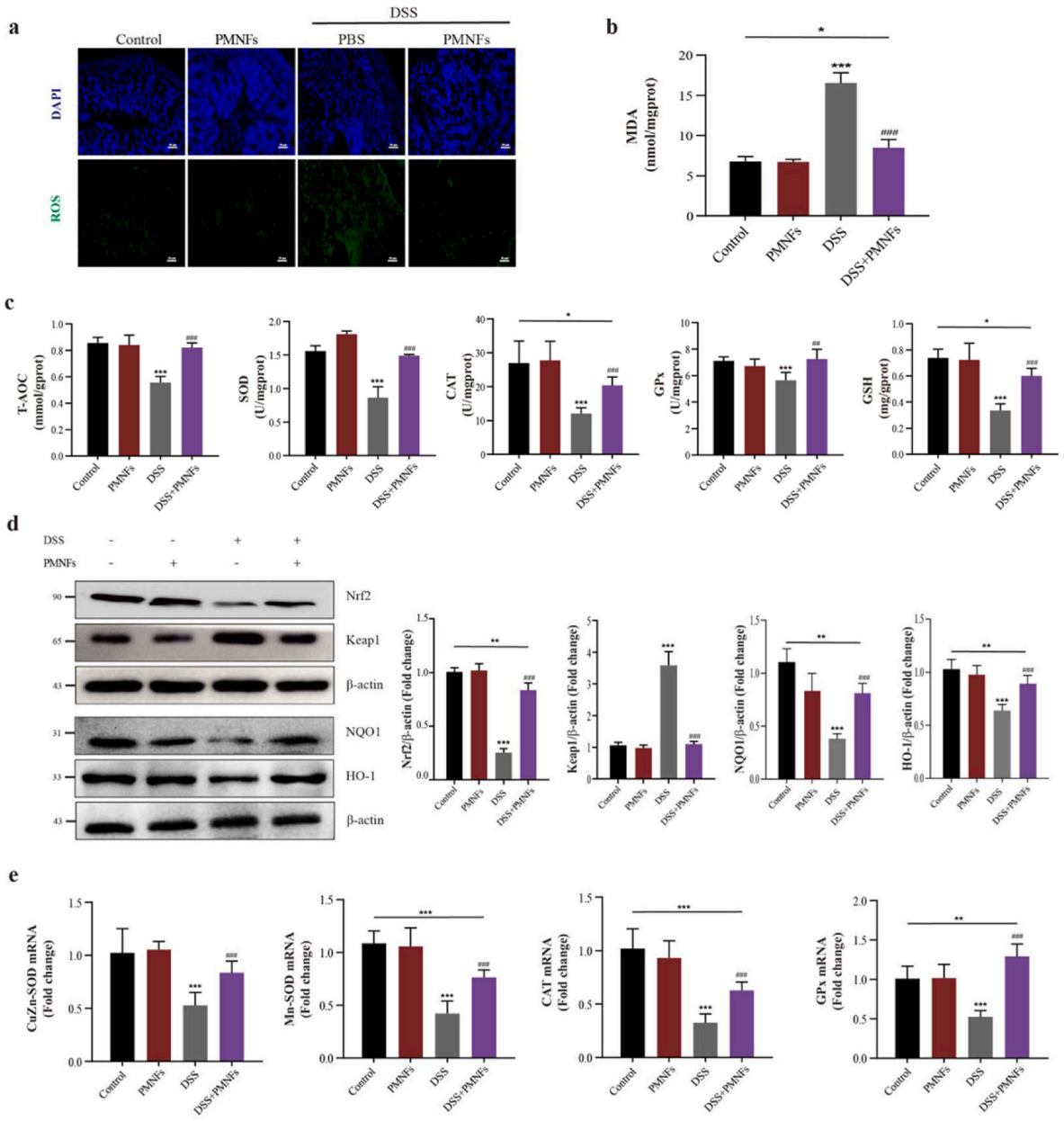


**Fig. 4.** PMNFs inhibits oxidative damage induced by DSS in the colon of mice. (a) Relative ROS amounts determined by DCFH-DA staining in the colon. Scale bars, 50 μm. (b) MDA content in the colon. (c) Antioxidant enzyme T-AOC, CAT, GPx and SOD activity and GSH content in the colon. (d) Western blot analysis of Nrf2, Keap1, NQO1 and HO-1 levels in the colon and the quantification data. (e) The expression of mRNA for CuZn-SOD, Mn-SOD, CAT and GPx in the colon, detected by qRT-PCR. For all quantifications, data (mean ± SD) were from the indicated number of independent experiments and analyzed with two-way ANOVA. *P < 0.05, **P < 0.01, ***P < 0.001 versus the control group; #P < 0.05, ##P < 0.01, ###P < 0.001 versus DSS-induced colitis group.

system.

### 3.6. PMNFs against inflammation though inhibiting TLR4/NF-κB pathway

Next, the effects of PMNFs on inflammatory responses of DSS-induced UC were investigated. The results in Fig. 5a and b showed that the pro-inflammatory cytokines IL-1β, IL-6, TNF-α and IFN-β levels in serum and in colonic significantly increased by DSS triggering, but the supplementation of PMNFs effectively inhibited the effect of DSS and controlled the growth of the pro-inflammatory cytokines content. Consistent with this, co-treatment mice with PMNFs visibly ablated enhanced IL-1β, IL-6, TNF-α and IFN-β mRNA expression by DSS (Fig. 5c). In addition, the involvement of Toll-like receptor 4 (TLR4)/nuclear factor-kappaB (NF-κB) pathway was closely related to the inflammatory response in UC, and even played a key role [34,35]. NF-κB is a kind of proteins bound and inhibited by IκBα proteins in normal condition, which is closely related to the occurrence of inflammation [36]. TLR4 is a vital pattern recognition receptor, and it is able to identify pathogenic bacteria that transpose into the blood circulation, thereby initiating downstream signal transduction pathways and ultimately activating NF-κB pathway [36]. In Fig. 5c and d, the increase in TLR4 and p–NF–κB protein levels and decrease in IκBα protein level indicate that TLR4/NF-κB pathway was activated in DSS-induced colitis mice. In contrast, co-treatment PMNFs can reverse the result caused by DSS.

RAW264.7 cells were employed to investigate anti-inflammatory activity of PMNFs in vitro. After pre-treating with PMNFs for 2 h, the

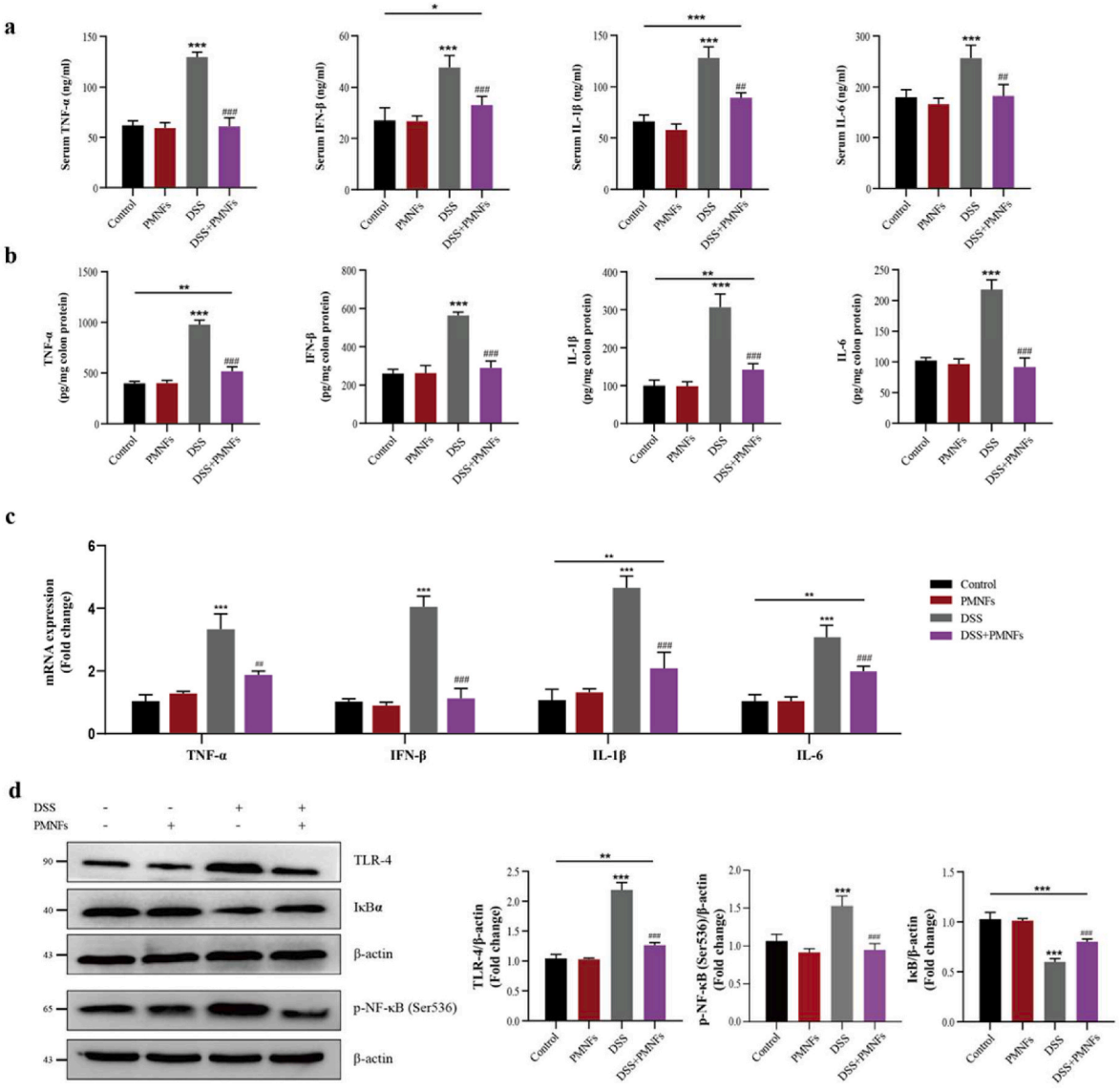


**Fig. 5.** PMNFs inhibits inflammation induced by DSS in the colon of mice. (a) Serum pro-inflammatory cytokines IL-1β, IL-6, TNF-α and IFN-β contents, detected by ELISA. (b) Pro-inflammatory cytokines IL-1β, IL-6, TNF-α and IFN-β contents in the colon, detected by ELISA. (c) The expression of IL-1β, IL-6, TNF-α and IFN-β mRNA levels in the colon, detected by qRT-PCR. (d) Western blot analysis of TLR4, p–NF–κB (Ser536) and IκBα levels in the colon and the quantification data. For all quantifications, data (mean ± SD) were from the indicated number of independent experiments and analyzed with two-way ANOVA. *P < 0.05, **P < 0.01, ***P < 0.001 versus the control group; #P < 0.05, ##P < 0.01, ###P < 0.001 versus DSS-induced colitis group.

cells were further stimulated with LPS for 6 h. PMNFs suppressed inflammation induced by LPS in dose-dependent manner (Figs. S7a, b, c). Through the comparison with the LPS group, there is a significant decrease in the protein levels and mRNA expression of pro-inflammatory cytokines (IL-1β, IL-6, TNF-α and IFN-β) for the DSS + PMNFs group, which is shown in Fig. 6a and b respectively. In addition, Fig. 6c shows that PMNFs also have anti-inflammatory effect on LPS-induced inflammation because PMNFs can inhibit the activation of LPS-induced TLR4/NF-κB pathway. And, the LPS triggered nucleus translocation of NF-κB was also suppressed by PMNFs (Fig. 6d) in RAW264.7 cells. Taken together, the anti-inflammatory activity of PMNFs should be mainly manifested by inhibiting activation of TLR4/NF-κB.

### *3.7. PMNFs protects against DSS-induced colitis though maintaining intestine barrier*

According to the former research results, the dysfunction of intestinal epithelial mechanical barrier is necessary pathological changes of UC [37,38]. Mucin-2 (MUC-2) is the most abundant mucus protein secreted by goblet cells. Compared with the results in DSS group, treatment with PMNFs lead to an increase in the expression of MUC-2 (Fig. 7a), which can maintain the integrity of the colonic mucous layer and protect the goblet cells [39,40]. Mice in the DSS-treated group exhibited a reduction of goblet cell, whereas PMNFs treatment markedly increased it (Fig. 7b). In addition, the TUNEL staining results indicated that PMNFs has the ability to prevent the DSS-induced apoptosis in the colon (Fig. 7c).

Consist with above studies, there is a significant decrease in tight junction (TJ) proteins (claudin-1, occludin, and ZO-1) for the mice in DSS-treated group, but the results in the group with PMNFs treatment show that PMNFs repaired the expression of these three proteins (Fig. 7d, e, f), which resulted the restoration of the integrity of the intestinal mucosal barrier. Taken these results together, it can be concluded that the inhibition of DSS-induced colitis by PMNFs was also related to its protection of the epithelial and mucosal barrier.

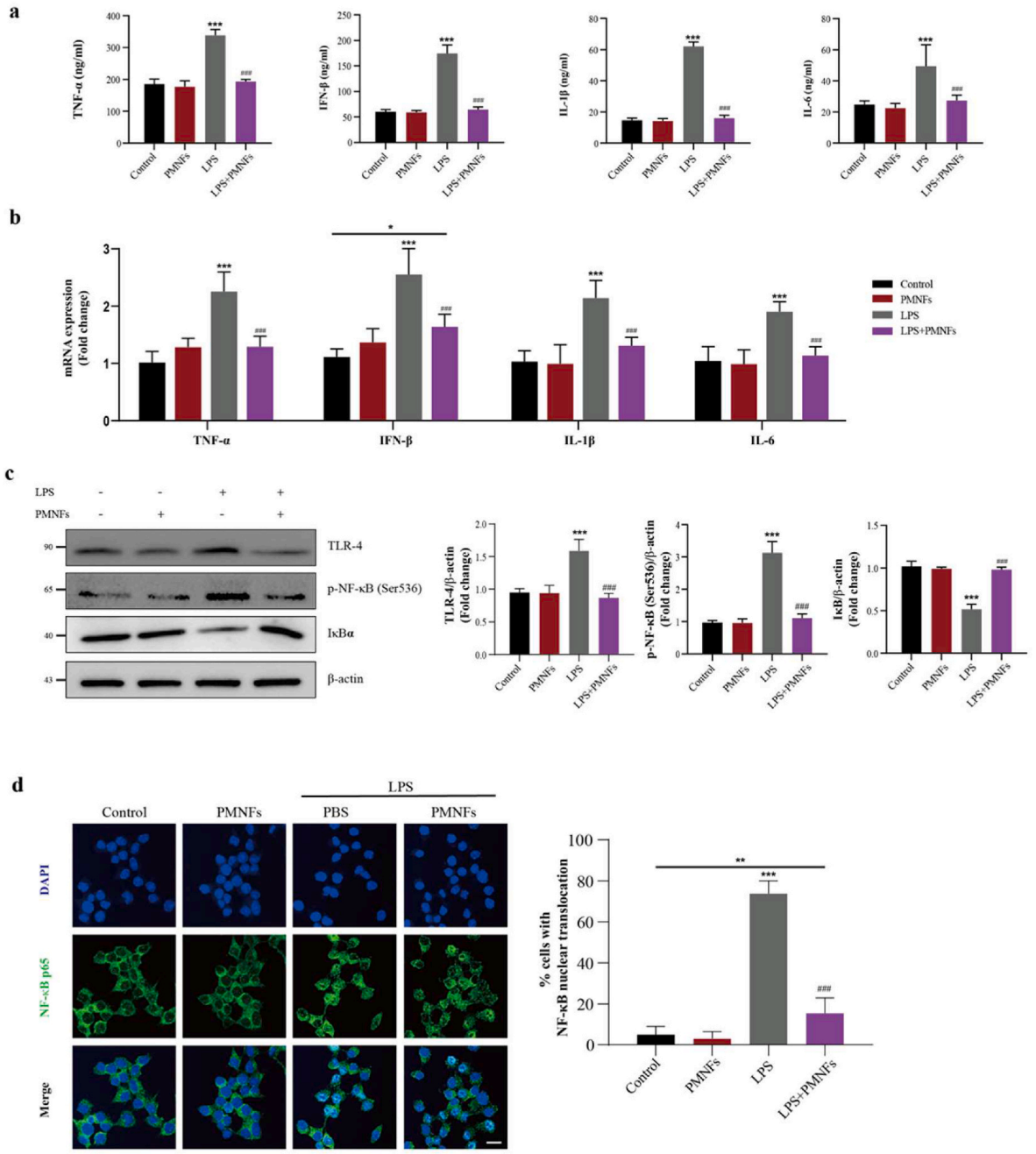


**Fig. 6.** PMNFs inhibits inflammation induced by LPS in RAW264.7 Macrophages. (a) Cell culture supernatant pro-inflammatory cytokines IL-1β, IL-6, TNF-α and IFN-β contents, detected by ELISA. (b) The expression of IL-1β, IL-6, TNF-α and IFN-β mRNA in RAW264.7 Macrophages, detected by qRT-PCR. (c) Western blot analysis of TLR4, p–NF–κB (Ser563) and IκBα and the quantification data in RAW264.7 Macrophages. (d) The translocation of NF-κB p65 protein from cytoplasm to nucleus in RAW264.7 Macrophages. For all quantifications, data (mean ± SD) were from the indicated number of independent experiments and analyzed with two-way ANOVA. *P < 0.05, **P < 0.01, ***P < 0.001 versus the control group; #P < 0.05, ##P < 0.01, ###P < 0.001 versus LPS treatment group.

## 4. Discussion

UC attracts more attention due to its increasing morbidity and the limitation of its specific drug, and it is difficult to diagnose in its early stages [41]. Exploring novel UC treatment drug is urgently needed in present research. Owing to its high efficiency, stability, and inexpensive, nanozyme have already been applied in many fields, such as food, medicine, agriculture, and so on [11]. Previous studies have reported that nanozyme, such as cerium oxide ($CeO_2$) nanoparticles, iron oxide (FeO) nanoparticles and manganese oxide nanoparticles, can inhibit the action of inflammatory mediators, thus protect the cellular structures from the destruction of inflammatory diseases [42]. In addition, it is reported that overload ROS production participates in the emergence of inflammation and promoted its development [43]. In this study, a new nanozyme $Mo_3Se_4$ nano flakes (PMNFs) was synthesized, and, the synthesized method was green, rapid, and cost-effective. PMNFs nanozyme was in the form of sheets with obvious aggregation distribution. The characterization of PMNFs was stable, good biocompatibility and water solubility, and blue fluorescence. Next, the results showed that PMNFs had ROS scavenging ability, including $H_2O_2$, $O_2^-$, and •OH. Previous studies have demonstrated that the antioxidant concentration of others metal-based nano-antioxidants (such as molybdenum-based composite materials, Ag, $CeO_2$ and CuO) are in the range of 0.5–5 mg/mL in vitro [44,45]. However, the antioxidant effect of PMNFs was 0.2–0.5 μg/mL,

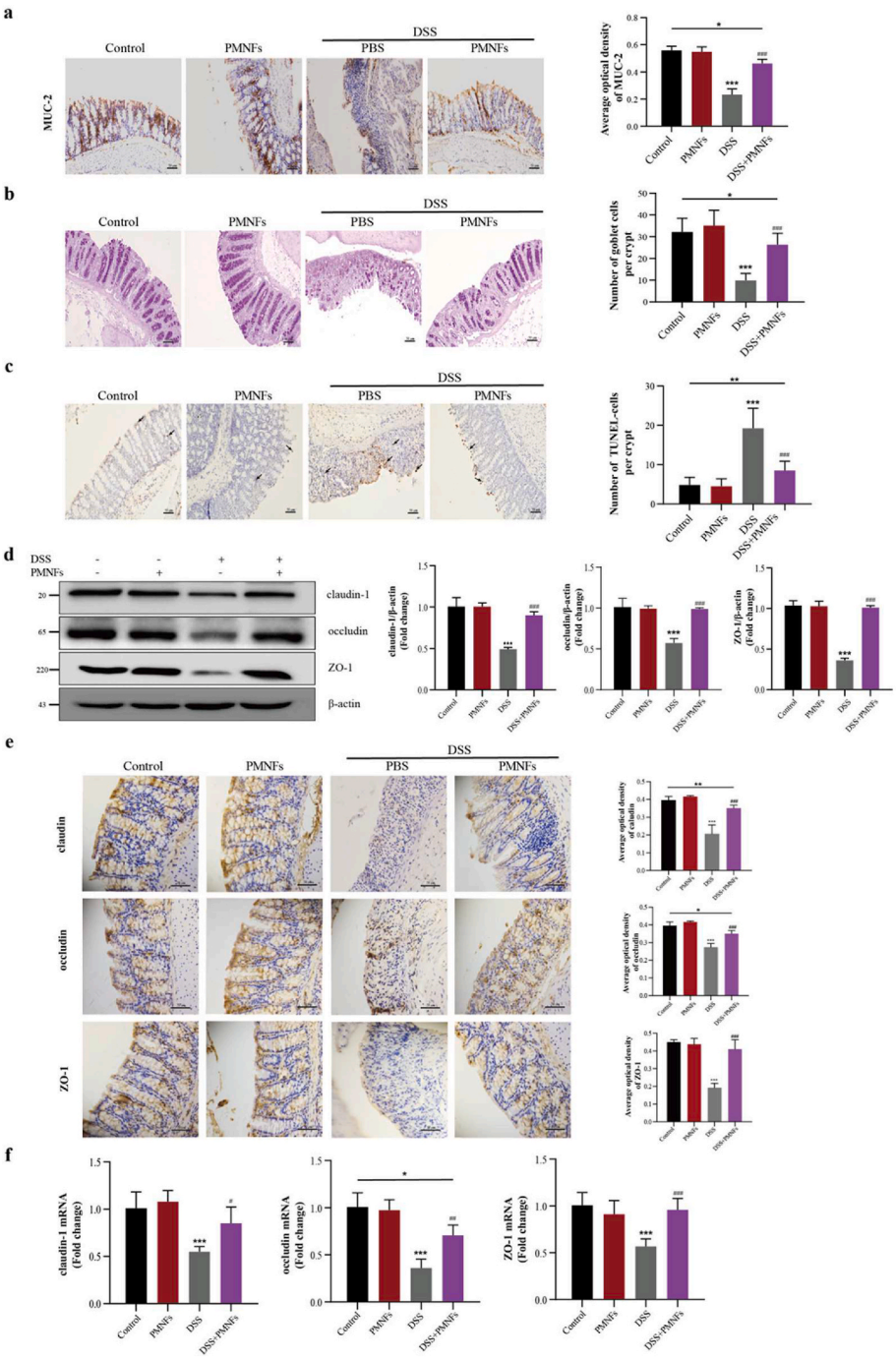


**Fig. 7.** PMNFs ameliorates intestinal barrier breakdown induced by DSS in the colon of mice. (a) IHC staining of MUC-2 in the colon and the quantification of MUC-2. Scale bars, 50 μm. (b) Representative image of goblet cells in the colon as determined by PAS staining and the quantification numbers of goblet cells. Scale bars, 50 μm. (c) Representative image of apoptosis in the colon as determined by TUNEL staining and the quantification numbers of apoptotic cells per group. Arrows denote cells undergoing apoptosis. Scale bars, 50 μm. (d) Western blot analysis of claudin-1, occludin and ZO-1 and the quantification data in the colon. (e) IHC staining and the quantification of claudin-1, occludin and ZO-1 in the colon. Scale bars, 50 μm. (f) The mRNA expression of claudin-1, occludin and ZO-1 in the colon, detected by qRT-PCR. For all quantifications, data (mean ± SD) were from the indicated number of independent experiments and analyzed with two-way ANOVA. *P < 0.05, **P < 0.01, ***P < 0.001 versus the control group; #P < 0.05, ##P < 0.01, ###P < 0.001 versus DSS-induced colitis group.

which was significantly lower than others metal-based nanozyme. Moreover, our results confirmed that PMNFs had multi-enzyme activities, such as CAT, GPx and SOD. Interesting, the SOD-like activity of PMNFs was almost more than two times than the natural SOD [20]. According to the good antioxidant ability of PMNFs, the application of PMNFs for UC therapy was explored in present research. An UC mice model was established by DSS, and, PMNFs was co-treatment by intragastric administration. Indeed, co-treatment with $MoSe_2$ showed a significantly decreased the clinical symptoms of DSS-induced colitis, including reducing DAI scores, body weight loss, shortening of the colon and histopathological abnormalities. Meanwhile, PMNFs treatment inhibited colonic MPO activity, which is a glycosylase present in neutrophil and monocyte granules and can be acts as a biological marker to assess the disease status of UC. These data indicate that PMNFs have efficiently suppression effect in DSS-induced colitis. Next, the potential mechanism of $MoSe_2$-attenuated DSS-induced colitis was explored, including oxidative stress, inflammation and intestine barrier.

Oxidative damage is the basic mechanism of several disease including the UC [5,33]. It has confirmed that oxidative stress is involved in the progression of inflammation, endothelial dysfunction, apoptosis, autophagy, cell migration, fibrosis and carcinogenesis. In inflammation disease, ROS or oxygen free radicals could promote the release of cytokines and chemokines, which induce epithelial cell apoptosis or necrosis and impair intestinal mechanical barrier [46]. The imbalance between ROS production and antioxidant capacity is the reason for oxidative stress [47]. Several researches have reported that removal of ROS could suggested to be an effective and preventive strategy against UC [48–50]. The anti-oxidative capacity of PMNFs has

been confirmed in the vitro study, whether it also can scavenge ROS in vivo is still unclear. PMNFs treatment inhibited the oxidative damage in the colon induced by DSS, including decrease in ROS and MDA and increase in anti-oxidative enzyme (T-AOC, CAT, GPx, and SOD) activities and GSH levels. Furthermore, in the LPS-primed RAW 264.7 macrophages, PMNFs also can scavenge the ROS. These results showed that the nanozyme activity of PMNFs was still very stable in the body and cell. Moreover, to discover the molecular mechanisms that might underlie the antioxidant effect of PMNFs, Nrf2-keap1 signaling pathway were measured. Nrf2-keap1 signaling pathway is an important defense mechanism in oxidative stress. Nrf2, an intracellular transcription factor, is combined with cytoplasmic Keap1 and degraded by Keap1 in normal conditions. In response to oxidative stress, Nrf2-Keap1 combination is dissociated, then Nrf2 is released and translocated to the nucleus, where it regulates the anti-oxidative- and anti-inflammation-related genes [51]. NQO1 and HO-1 are the main downstream of Nrf2-Keap1 pathway. It has reported that Nrf2-Keap1 signaling pathway is participated in the UC development. In UC mice model, DSS treatment inhibit Nrf2 levels and increased Keap1 levels, indicating Nrf2-Keap1 pathway is blocked [52]. And, several studies also explore whether Nrf2-Keap1 signaling pathway could be a prevention target for the drug research and development of UC [53]. Interesting, the Nrf2-keap1 signaling pathway was activated by PMNFs treatment. Moreover, in the present research, the inhibited expressions of Nrf2-targeted molecules (HO-1 and NQO-1) by DSS were significantly reversed after co-administered with PMNFs. In summary, the anti-oxidative activity of PMNFs should be mediated by directly scavenging ROS and the reconstitution of the Nrf2-mediated cellular anti-oxidative system.

When the inflammation of intestinal mucosa is uncontrolled and highly activated, the dynamic balance between intestinal antigens and host immunity can be disrupted [41], so that it finally evolved into UC [54]. Pro-inflammatory cytokine responses are an important pathophysiological factor which controls the occurrence and development of UC [54]. Our results showed that after PMNFs treatment, pro-inflammatory cytokines IL-1β, IL-6, TNF-α and IFN-β levels in serum and in colon were significantly suppressed. TLR4-mediated NF-κB activation plays a critical role in pro-inflammatory cytokines production in UC [55]. TLR4 is a key receptor for intestinal innate immune synesthesia and is increased in UC [8]. During inflammation, TLR4 is activated by recognition of pathogen-associated molecular patterns (PAMPs), and then is recruited to the aptamer, leading to NF-κB activation [56]. Activated NF-κB leads to the production of a variety of pro-inflammatory mediators. In this study, the TLR4/NF-κB pathway was activated in DSS-induced colitis, and, PMNFs treatment significantly suppressed TLR4/NF-κB pathway by decreasing TLR4 and p–NF–κB expression levels. Otherwise, for further verification the anti-inflammation of PMNFs, the effects of PMNFs on pro-inflammatory responses of LPS-stimulated macrophage are investigated. Consistent with the vivo study, PMNFs also prevented LPS-induced inflammation through TLR4/NF-κB pathway suppression in the macrophages.

The intestine barrier is very important for intestinal health and immunology, and it acts as a mechanical barrier to prevent the translocation of harmful substances from lumen to the inner [57]. The injure of intestinal mucosal barrier results in the infiltration of hazardous substances, including toxins, pathogens and antigens, from the lumen into the mucosal tissue. Thus, these hazardous substances cause inflammatory responses and tissue damage in the intestinal mucosa and even submucosa, leading to colitis [37]. The intestinal epithelial mechanical barrier includes a mucous layer and an epithelial cells layer [39]. It is not clear whether PMNFs could protect the intestinal epithelial mechanical barrier. In this research, the mucous layer and the epithelial cells layer was impaired in the colon of colitis mice. PMNFs treatment increased the expression of MUC-2 and the number of goblet cells. Meanwhile, the TUNEL staining results indicated that PMNFs had the ability to prevent the DSS-induced apoptosis in the colon. The function of mucous layer is to prevent the adhesion of lumen bacteria in the intestinal epithelium, simultaneously, the mucus proteins have antibacterial ability. TJ proteins play a vital role in the maintenance of the intestinal epithelial barrier. The increase in permeability of TJs can directly enhance the pathogenesis of UC [3,58]. TJs are composed with multiprotein complexes, including the cytoplasmic proteins, occludin, ZO-1, and claudins [59]. ZO proteins play an important part in epithelial cellular permeability and adhesion, TJ formation and stabilization, and signal transmission. Occludin acts as an important part in TJs assembly and disassembly, then regulates the permeability of intestinal epithelial. Claudin, as a skeletal protein, builds the basement membrane of TJs. Consist with above studies, there is a significant decrease in claudin-1, occludin, and ZO-1 for the mice in DSS-treated group, but, PMNFs treatment can restore them.

## 5. Conclusion

In conclusion, as a novel nanozyme, PMNFs have multi-enzyme activity with CAT, SOD, GPx in *vitro*, and the antioxidant effect of PMNFs was higher than others metal-based nanozymes. Meanwhile, PMNFs could efficiently alleviate colitis symptoms induced by DSS. In *vivo* study, PMNFs also could directly scavenge the ROS, moreover, PMNFs treatment increase antioxidant activity through activation of antioxidant pathway Nrf2-keap1 signal. In addition, PMNFs suppress the expression of pro-inflammatory cytokines via the inactivation of TLR4/NF-κB pathway in both colonic tissues stimulated by DSS and LPS-primed macrophage. Furthermore, PMNFs can maintain intestine barriers through upregulation of TJ proteins and MUC-2, and amelioration epithelial apoptosis. In a word, PMNFs show its unique role in inhibiting colitis and it had potential application value for the treatment of various diseases caused by oxidative stress.

## Credit authorship contribution statement

Hongrui Guo: Conceptualization, Experiment design, Writing – review & editing, Funding acquisition. Hai Guo: Experimental section, Data Formal analysis, Writing – original draft. Yue Xie: Experimental section, Data Formal analysis. Yinyin Chen: Experimental section, Data Formal analysis. Changfang Lu: Writing – review & editing. Zhouping Yang: Writing – review & editing. Yanqiu Zhu: Data analysis. Yujuan Ouyang: Experimental section, Data Formal analysis. Yu Zhang: Data analysis. Xianxiang Wang: Conceptualization, Experiment design, Writing – review & editing, Funding acquisition.

## Declaration of competing interest

The authors declare no conflict of interest.

## Data availability

Data will be made available on request.

## Acknowledgements

The authors thank the financial support of this work by the Sichuan Science and Technology Program (Grant No. 2020YJ0113), the National Natural Science Foundation of China (Grant No. 21305097).

## Appendix A. Supplementary data

Supplementary data to this article can be found online at https://doi.org/10.1016/j.redox.2022.102441.

## References


[1] D.B. Graham, R.J. Xavier, Pathway paradigms revealed from the genetics of inflammatory bowel disease, Nature 578 (7796) (2020) 527–539.
[2] R. Ungaro, S. Mehandru, P.B. Allen, L. Peyrin-Biroulet, J.-F. Colombel, Ulcerative colitis, Lancet 389 (10080) (2017) 1756–1770.
[3] Y. Cao, J.Z. Gao, L.H. Zhang, N.B. Qin, B.W. Zhu, X.D. Xia, Jellyfish skin polysaccharides enhance intestinal barrier function and modulate the gut microbiota in mice with DSS-induced colitis, Food Funct. 12 (20) (2021) 10121–10135.
[4] I. Ordás, L. Eckmann, M. Talamini, D.C. Baumgart, W.J. Sandborn, Ulcerative colitis, Lancet 380 (9853) (2012) 1606–1619.
[5] J. Hwang, J. Jin, S. Jeon, S.H. Moon, M.Y. Park, D.Y. Yum, J.H. Kim, J.E. Kang, M. H. Park, E.J. Kim, J.G. Pan, O. Kwon, G.T. Oh, SOD1 suppresses pro-inflammatory immune responses by protecting against oxidative stress in colitis, Redox Biol. 37 (2020), 101760.
[6] J. Huang, J. Zhang, J. Ma, J. Ma, J. Liu, F. Wang, X. Tang, Inhibiting ferroptosis: a novel approach for ulcerative colitis therapeutics, Oxid. Med. Cell. Longev. 2022 (2022), 9678625.
[7] N. Tahvilian, M. Masoodi, A. Faghihi Kashani, M. Vafa, N. Aryaeian, A. Heydarian, A. Hosseini, N. Moradi, F. Farsi, Effects of saffron supplementation on oxidative/antioxidant status and severity of disease in ulcerative colitis patients: a randomized, double-blind, placebo-controlled study, Phytother Res. 35 (2) (2021) 946–953.
[8] Y. Qu, X. Li, F. Xu, S. Zhao, X. Wu, Y. Wang, J. Xie, Kaempferol alleviates murine experimental colitis by restoring gut microbiota and inhibiting the LPS-TLR4-NF-κb Axis, Front. Immunol. 12 (2021), 679897.
[9] M. Zhang, D. Merlin, Nanoparticle-based oral drug delivery systems targeting the colon for treatment of ulcerative colitis, Inflamm. Bowel Dis. 24 (7) (2018) 1401–1415.
[10] M. Chen, Y. Ding, Z. Tong, Efficacy and safety of Sophora flavescens (Kushen) based traditional Chinese medicine in the treatment of ulcerative colitis: clinical evidence and potential mechanisms, Front. Pharmacol. 11 (2020), 603476.
[11] J. Wu, X. Wang, Q. Wang, Z. Lou, S. Li, Y. Zhu, L. Qin, H. Wei, Nanomaterials with enzyme-like characteristics (nanozymes): next-generation artificial enzymes (II), Chem. Soc. Rev. 48 (4) (2019) 1004–1076.
[12] Y. Chen, H. Zou, B. Yan, X. Wu, W. Cao, Y. Qian, L. Zheng, G. Yang, Atomically dispersed Cu nanozyme with intensive ascorbate peroxidase mimic activity capable of alleviating ROS-mediated oxidation damage, Adv. Sci. 9 (5) (2022).
[13] S. Gao, H. Lin, H. Zhang, H. Yao, Y. Chen, J. Shi, Nanocatalytic tumor therapy by biomimetic dual inorganic nanozyme-catalyzed cascade reaction, Adv. Sci. 6 (3) (2019).
[14] M. Parra-Robert, M. Zeng, Y. Shu, G. Fernández-Varo, M. Perramón, D. Desai, J. Chen, D. Guo, X. Zhang, M. Morales-Ruiz, J.M. Rosenholm, W. Jiménez, V. Puntes, E. Casals, G. Casals, Mesoporous silica coated CeO2 nanozymes with combined lipid-lowering and antioxidant activity induce long-term improvement of the metabolic profile in obese Zucker rats, Nanoscale 13 (18) (2021) 8452–8466.
[15] J.C. Barreto, G.S. Smith, N.H. Strobel, P.A. McQuillin, T.A. Miller, Terephthalic acid: a dosimeter for the detection of hydroxyl radicals in vitro, Life Sci. 56 (4) (1995) Pl89–96.
[16] J.C. Barreto, G.S. Smith, N.H.P. Strobel, P.A. McQuillin, T.A. Miller, Terephthalic acid - a dosimeter for the detection df hydroxyl radicals in-vitro, Life Sci. 56 (4) (1994) PL89–PL96.
[17] D. Yim, D.E. Lee, Y. So, C. Choi, W. Son, K. Jang, C.S. Yang, J.H. Kim, Sustainable nanosheet antioxidants for sepsis therapy via scavenging intracellular reactive oxygen and nitrogen species, ACS Nano 14 (8) (2020) 10324–10336.
[18] H. Gu, X. Chen, F. Chen, X. Zhou, Z. Parsaee, Ultrasound-assisted biosynthesis of CuO-NPs using brown alga Cystoseira trinodis: characterization, photocatalytic AOP, DPPH scavenging and antibacterial investigations, Ultrason. Sonochem. 41 (2018) 109–119.
[19] P. Xie, L. Zhang, H. Shen, H. Wu, J. Zhao, S. Wang, L. Hu, Biodegradable MoSe2-polyvinylpyrrolidone nanoparticles with multi-enzyme activity for ameliorating acute pancreatitis, J. Nanobiotechnol. 20 (1) (2022) 113.
[20] X. Zhu, P. Liu, Y. Ge, R. Wu, T. Xue, Y. Sheng, S. Ai, K. Tang, Y. Wen, MoS2/MWCNTs porous nanohybrid network with oxidase-like characteristic as electrochemical nanozyme sensor coupled with machine learning for intelligent analysis of carbendazim, J. Electroanal. Chem. 862 (2020).
[21] Y. Peng, Y. Ren, H. Zhu, Y. An, B. Chang, T.J.R.A. Sun, Ultrasmall copper nanoclusters with multi-enzyme activities 11 (24) (2021) 14517–14526.
[22] W. Yin, J. Yu, F. Lv, L. Yan, L.R. Zheng, Z. Gu, Y. Zhao, Functionalized nano-MoS2 with peroxidase catalytic and near-infrared photothermal activities for safe and synergetic wound antibacterial applications, ACS Nano 10 (12) (2016) 11000–11011.
[23] Z. Liu, L. Xie, K. Qiu, X. Liao, T.W. Rees, Z. Zhao, L. Ji, H.J.A.A.M. Chao, Interfaces, An ultrasmall RuO2 nanozyme exhibiting multienzyme-like activity for the prevention of acute kidney injury 12 (28) (2020) 31205–31216.
[24] C. Quach, Y. Song, H. Guo, S. Li, H. Maazi, in: A Truncating Mutation in the Autophagy Gene UVRAG Drives Inflammation and Tumorigenesis in Mice, vol. 10, 2019, p. 5681 (1).
[25] H. Guo, Y. Ouyang, J. Wang, H. Cui, H. Deng, X. Zhong, Z. Jian, H. Liu, J. Fang, Z. Zuo, X. Wang, L. Zhao, Y. Geng, P. Ouyang, H. Tang, Cu-induced spermatogenesis disease is related to oxidative stress-mediated germ cell apoptosis and DNA damage, J. Hazard Mater. 416 (2021), 125903.
[26] Y.H. Seon, Y.C. Kang, J.S. Cho, One-dimensional porous nanostructure composed of few-layered MoSe2 nanosheets and highly densified-entangled-N-doped CNTs as anodes for Na ion batteries, Chem. Eng. J. 425 (2021) 15.
[27] J.S. Cho, J.-S. Park, K.M. Jeon, Y.C.J.J.o.M.C.A. Kang, in: 1-D Nanostructure Comprising Porous Fe 2 O 3/Se Composite Nanorods with Numerous Nanovoids, and Their Electrochemical Properties for Use in Lithium-Ion Batteries, vol. 5, 2017, pp. 10632–10639 (21).
[28] T. Xiang, S. Tao, W. Xu, Q. Fang, C. Wu, D. Liu, Y. Zhou, A. Khalil, Z. Muhammad, W. Chu, Z. Wang, H. Xiang, Q. Liu, L. Song, Stable 1T-MoSe2 and carbon nanotube hybridized flexible film: binder-free and high-performance Li-ion anode, ACS Nano 11 (6) (2017) 6483–6491.
[29] H. Mittal, M. Khanuja, Hydrothermal in-situ synthesis of MoSe2-polypyrrole nanocomposite for efficient photocatalytic degradation of dyes under dark and visible light irradiation, Separ. Purif. Technol. 254 (2021) 13.
[30] M. Hosseini, F. Sadat Sabet, H. Khabbaz, M. Aghazadeh, F. Mizani, M.R. Ganjali, Enhancement of the peroxidase-like activity of cerium-doped ferrite nanoparticles for colorimetric detection of H2O2 and glucose, Anal. Methods 9 (23) (2017) 3519–3524.
[31] D. Jampaiah, T. Srinivasa Reddy, A.E. Kandjani, P.R. Selvakannan, Y.M. Sabri, V. E. Coyle, R. Shukla, S.K. Bhargava, Fe-doped CeO2 nanorods for enhanced peroxidase-like activity and their application towards glucose detection, J. Mater. Chem. B 4 (22) (2016) 3874–3885.
[32] L. Gao, J. Zhuang, L. Nie, J. Zhang, Y. Zhang, N. Gu, T. Wang, J. Feng, D. Yang, S. Perrett, X. Yan, Intrinsic peroxidase-like activity of ferromagnetic nanoparticles, Nat. Nanotechnol. 2 (9) (2007) 577–583.
[33] K.P. Pavlick, F.S. Laroux, J. Fuseler, R.E. Wolf, L. Gray, J. Hoffman, M.B. Grisham, Role of reactive metabolites of oxygen and nitrogen in inflammatory bowel disease, Free Radic. Biol. Med. 33 (3) (2002) 311–322.
[34] J.-C. Lin, J.-Q. Wu, F. Wang, F.-Y. Tang, J. Sun, B. Xu, M. Jiang, Y. Chu, D. Chen, X. Li, S. Su, Y. Zhang, N. Wu, S. Yang, K. Wu, J. Liang, QingBai decoction regulates intestinal permeability of dextran sulphate sodium-induced colitis through the modulation of notch and NF-κB signalling, Cell Prolif 52 (2) (2019), e12547.
[35] S. Qiu, P. Li, H. Zhao, X. Li, Maresin 1 alleviates dextran sulfate sodium-induced ulcerative colitis by regulating NRF2 and TLR4/NF-kB signaling pathway, Int. Immunopharm. 78 (2020), 106018.
[36] S. Mitchell, J. Vargas, A. Hoffmann, Signaling via the NFκB system, WIREs Syst. Biol. Med. 8 (3) (2016) 227–241.
[37] H. Zhang, Y. Wang, Y. Su, X. Fang, W. Guo, The alleviating effect and mechanism of Bilobalide on ulcerative colitis, Food Funct. 12 (14) (2021) 6226–6239.
[38] K. Parikh, A. Antanaviciute, D. Fawkner-Corbett, M. Jagielowicz, A. Aulicino, C. Lagerholm, S. Davis, J. Kinchen, H.H. Chen, N.K. Alham, N. Ashley, E. Johnson, P. Hublitz, L. Bao, J. Lukomska, R.S. Andev, E. Björklund, B.M. Kessler, R. Fischer, R. Goldin, H. Koohy, A. Simmons, Colonic epithelial cell diversity in health and inflammatory bowel disease, Nature 567 (7746) (2019) 49–55.
[39] G.P. Ramos, K.A. Papadakis, Mechanisms of disease: inflammatory bowel diseases, Mayo Clin. Proc. 94 (1) (2019) 155–165.
[40] M. Van der Sluis, B.A. De Koning, A.C. De Bruijn, A. Velcich, J.P. Meijerink, J. B. Van Goudoever, H.A. Büller, J. Dekker, I. Van Seuningen, I.B. Renes, A. W. Einerhand, Muc2-deficient mice spontaneously develop colitis, indicating that MUC2 is critical for colonic protection, Gastroenterology 131 (1) (2006) 117–129.
[41] G.G. Kaplan, S.C. Ng, Understanding and preventing the global increase of inflammatory bowel disease, Gastroenterology 152 (2) (2017) 313–321.e2.
[42] H.J. Wang, Z.C. Cui, X. Wang, S. Sun, D.S. Zhang, C.A.Y. Fu, Therapeutic applications of nanozymes in chronic inflammatory diseases, BioMed Res. Int. 2021 (2021).
[43] S. Chen, X. Wu, Z. Yu, Juglone suppresses inflammation and oxidative stress in colitis mice, Front. Immunol. 12 (2021), 674341.
[44] J. Kaur, K. Kaur, S.K. Mehta, A.S. Matharu, A novel molybdenum oxide–Starbon catalyst for wastewater remediation, J. Mater. Chem. 8 (29) (2020) 14519–14527.
[45] H. Gu, X. Chen, F. Chen, X. Zhou, Z. Parsaee, Ultrasound-assisted biosynthesis of CuO-NPs using brown alga Cystoseira trinodis: characterization, photocatalytic AOP, DPPH scavenging and antibacterial investigations, Ultrason. Sonochem. 41 (2018) 109–119.
[46] Y. Chen, B. Yang, R.P. Ross, Y. Jin, C. Stanton, J. Zhao, H. Zhang, W. Chen, Orally administered CLA ameliorates DSS-induced colitis in mice via intestinal barrier improvement, oxidative stress reduction, and inflammatory cytokine and gut microbiota modulation, J. Agric. Food Chem. 67 (48) (2019) 13282–13298.
[47] H.A.A. Elmaksoud, M.H. Motawea, A.A. Desoky, M.G. Elharrif, A. Ibrahimi, Hydroxytyrosol alleviate intestinal inflammation, oxidative stress and apoptosis resulted in ulcerative colitis, Biomed. Pharmacother. 142 (2021), 112073.
[48] N. Zhao, F.E. Yang, C.Y. Zhao, S.W. Lv, J. Wang, J.M. Liu, Construction of pH-dependent Nanozymes with Oxygen Vacancies as the High-Efficient Reactive Oxygen Species Scavenger for Oral-Administrated Anti-inflammatory Therapy, 2021, e2101618.
[49] H. Xu, R. Luo, L. Dong, X. Pu, Q. Chen, N. Ye, S. Qi, X. Han, W. Nie, C. Fu, Y. Hu, J. Zhang, F. Gao, pH/ROS dual-sensitive and chondroitin sulfate wrapped poly (β-amino ester)-SA-PAPE copolymer nanoparticles for macrophage-targeted oral therapy for ulcerative colitis, Nanomedicine (2021), 102461.
[50] X. Yang, Z. Mao, Y. Huang, H. Yan, Q. Yan, J. Hong, J. Fan, J. Yao, Reductively modified albumin attenuates DSS-Induced mouse colitis through rebalancing systemic redox state, Redox Biol. 41 (2021), 101881.
[51] I. Bellezza, I. Giambanco, A. Minelli, R. Donato, Nrf2-Keap1 signaling in oxidative and reductive stress, Biochimica et biophysica acta, Mole. Cell Res. 1865 (5) (2018) 721–733.
[52] F. Guo, R. Tsao, C. Li, X. Wang, H. Zhang, L. Jiang, Y. Sun, H. Xiong, Green pea (pisum sativum L.) hull polyphenol extracts ameliorate DSS-induced colitis through keap1/nrf2 pathway and gut microbiota modulation, Foods 10 (11) (2021).

[53] C. Liu, H. Hua, H. Zhu, Y. Cheng, Y. Guo, W. Yao, H. Qian, Aloe polysaccharides ameliorate acute colitis in mice via Nrf2/HO-1 signaling pathway and short-chain fatty acids metabolism, Int. J. Biol. Macromol. 185 (2021) 804–812.
[54] R. Ungaro, S. Mehandru, P.B. Allen, L. Peyrin-Biroulet, J.F. Colombel, Ulcerative colitis, Lancet (London, England) 389 (10080) (2017) 1756–1770.
[55] J.L. Duan, H.Q. He, Y. Yu, T. Liu, S.J. Ma, F. Li, Y.S. Jiang, X. Lin, D.D. Li, Q.Z. Lv, H.H. Ma, X.M. Jia, E3 ligase c-Cbl regulates intestinal inflammation through suppressing fungi-induced noncanonical NF-κB activation, Sci. Adv. 7 (19) (2021).
[56] X. Liu, B. Lu, J. Fu, X. Zhu, E. Song, Y. Song, Amorphous silica nanoparticles induce inflammation via activation of NLRP3 inflammasome and HMGB1/TLR4/MYD88/NF-kb signaling pathway in HUVEC cells, J. Hazard Mater. 404 (Pt B) (2021), 124050.
[57] M. Alipour, D. Zaidi, R. Valcheva, J. Jovel, I. Martínez, C. Sergi, J. Walter, A. L. Mason, G.K. Wong, L.A. Dieleman, M.W. Carroll, H.Q. Huynh, E. Wine, Mucosal barrier depletion and loss of bacterial diversity are primary abnormalities in paediatric ulcerative colitis, J. Crohn's Colitis 10 (4) (2016) 462–471.
[58] T. Suzuki, Regulation of the intestinal barrier by nutrients: the role of tight junctions, Anim. Sci. J. 91 (1) (2020), e13357.
[59] C. Chelakkot, J. Ghim, S.H. Ryu, Mechanisms regulating intestinal barrier integrity and its pathological implications, Exp. Mol. Med. 50 (8) (2018) 1–9.